Chapter 3
RESULTS AND DISCUSSION

3.1 Characterization of activated carbons surfaces

3.1.1 Scanning electron microscopy (SEM)

The scanning electron micrographs of the external structures of two activated carbons, B-70-600 and Pr-70-600, are shown in Figure 2. It can be seen from micrographs that both samples are full of holes with diameters ranging from around 1-10 μm. These holes are defined as macropore of the activated carbons (> 50 nm). Even at higher magnification both micropore and mesopore cannot be resolved by scanning microscopy due to the limit of detection of instrument. This reason is the same for disadvantage in imaging of the rest of carbons, B-325-800 and Pr-325-800.

The formation of activated carbons obtained corresponds to Teng and Yeh (Teng and Yeh, 1998) who reported the occurrence of macropore in activated carbon obtained from bituminous coals with zinc chloride activation. The reason for the formation of the holes on the activated carbon is not clear. According to micrograph of Figure 2, it seems that the holes resulted from the evaporation of $ZnCl_2$ during activation, leaving the space previously occupied by $ZnCl_2$.

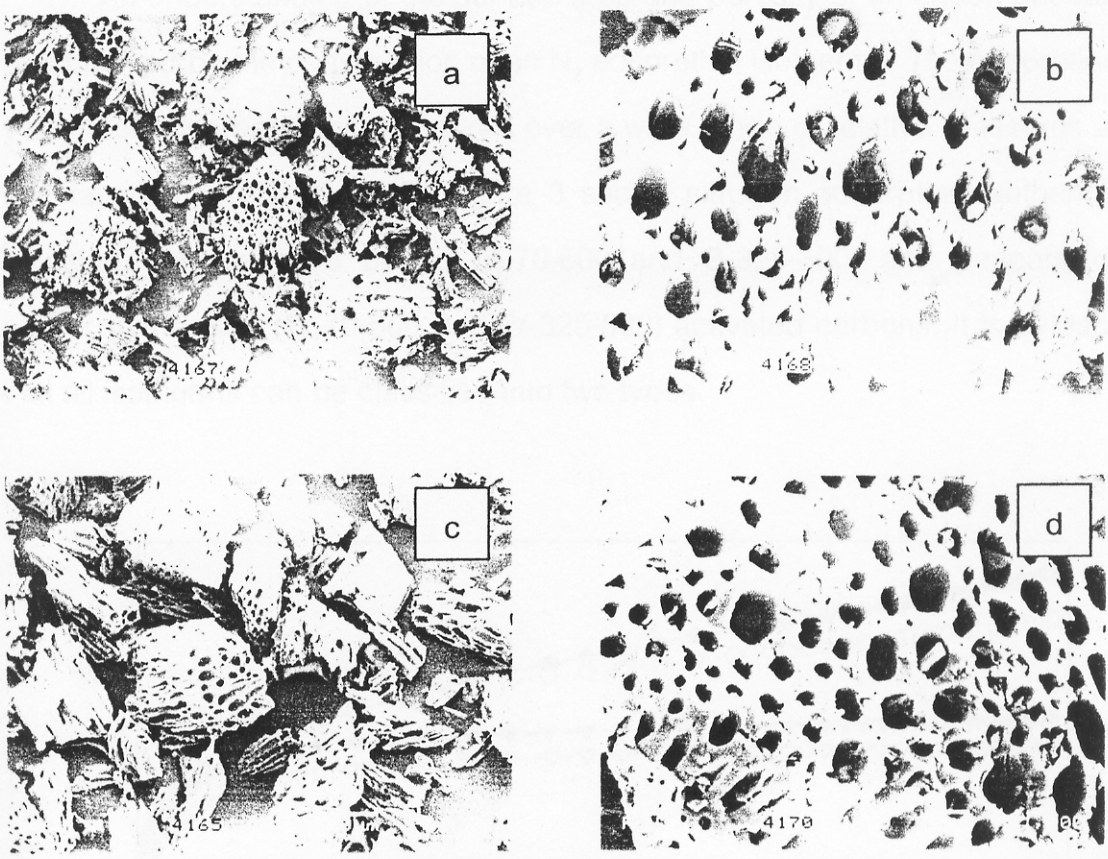

Figure 2 SEM micrographs of (a) B-70-600 (×150), (b) B-70-600 (×1000), (c) Pr-70-600 (×150), (d) Pr-70-600 (×1000) activated carbons.

SEM images of both B-70-600 and Pr-70-600 are similar. Therefore, it is reasonable to conclude that materials and the activation process do not effect to macropore or external structure of these samples. Although it is simplified to characterize external surface of the activated carbons, this method cannot be identified further information of smaller pores (micropore and mesopore).

3.1.2 Surface area and pore size analysis (physical or porous texture characterization

An understanding of the surface area and porosity of an adsorbent can be achieved by the construction of an N_2 adsorption isotherms. The adsorption volume of adsorbent was measured over a wide range of relative pressures at constant temperature (77 K). Figure 3 shows nitrogen adsorption isotherms measured on bagasse based (B-70-600 and B-325-800) and pericarp of rubber fruit based (Pr-70-600 and Pr-325-800) activated carbons. It is evident that all isotherms can be classified into two types.

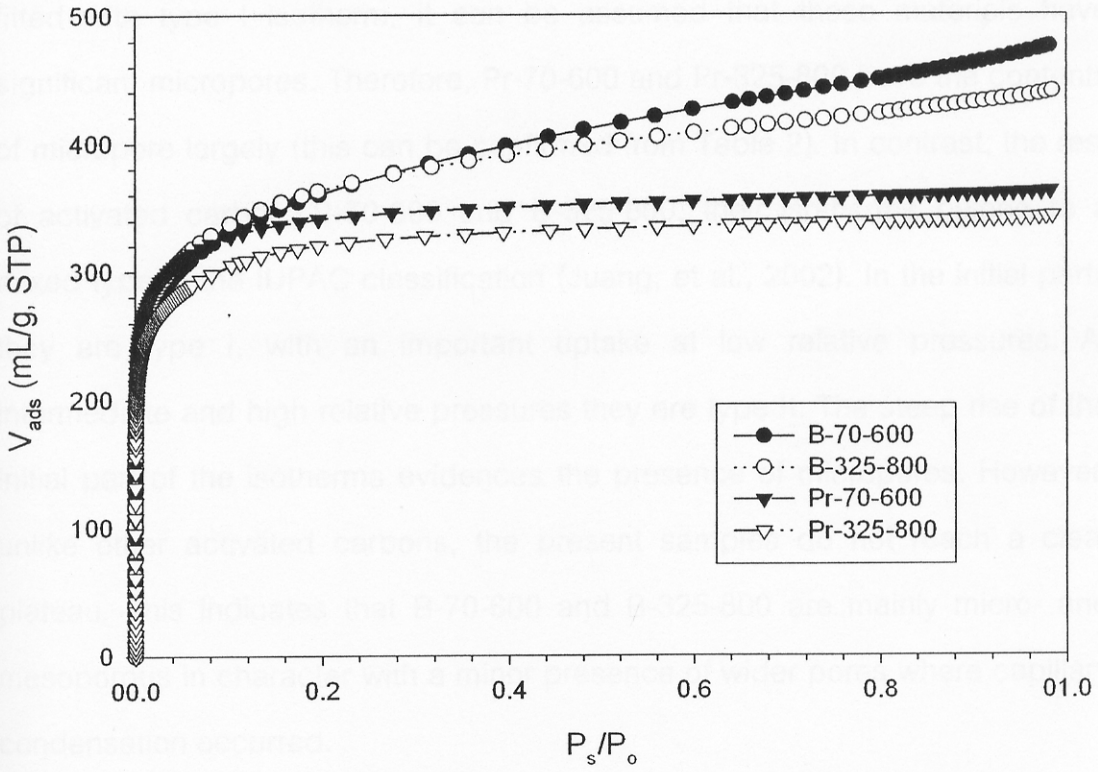

Figure 3 Adsorption isotherms of N_2 at 77 K on the carbons prepared from two agricultural wastes. (P_s/P_O is relative pressure).

In the case of Pr-70-600 and Pr-325-800, the samples are approximately Type I according to IUPAC classification (Hu and Vansant, 1995) since most of the adsorbed volume is contained in the micropores. These isotherms show the steep rise of the initial part of the isotherms where micropores is filled by nitrogen molecules completely at ~ 0.2 P/P_o. The isotherms become plateau after 0.2 P/P_o. It is now widely accepted that the initial part of the Type I isotherm represents micropore filling and that the slope of the plateau at high relative pressure is due to multilayer adsorption on the nonmicroporous structures, i.e., in mesopores, in macropores, and on the external surface. If nitrogen adsorption isotherm of any porous material can be fitted with type I isotherm, it can be assumed that those materials have significant micropores. Therefore, Pr-70-600 and Pr-325-800 have the contents of micropore largely (this can be confirmed from Table 2). In contrast, the rest of activated carbon, B-70-600 and B-325-800, their isotherms belong to a mixed type in the IUPAC classification (Juang, et al., 2002). In the initial parts they are type I, with an important uptake at low relative pressures. At intermediate and high relative pressures they are type II. The steep rise of the initial part of the isotherms evidences the presence of micropores. However, unlike other activated carbons, the present samples do not reach a clear plateau. This indicates that B-70-600 and B-325-800 are mainly micro- and mesoporous in character with a minor presence of wider pores where capillary condensation occurred.

Table 2 BET and micropore surface areas of activated carbons prepared from bagasse and pericarp of rubber fruit.

Samples	BET surface areas (m^2/g)	micropore surface areas (m^2/g)	micropore fractions (%)	micropore volumes (mL/g)
B-70-600	1274.23	630.85	49.51	0.2757
B-325-800	1279.82	736.63	57.56	0.3229
Pr-70-600	1187.02	913.62	76.97	0.4082
Pr-325-800	1128.01	807.53	71.59	0.3549

Further understanding in porous characters of all carbons can be observed from Table 2. The results show that all of the samples possess a well-developed porous structure. B-325-800 and B-70-600 exhibit similar BET surface areas and more slightly than the others (Pr-70-600 and Pr-325-800). Although there is the difference among BET surface area of the samples, it is less than 10%. So, BET surface areas may not affect the adsorption process in this study.

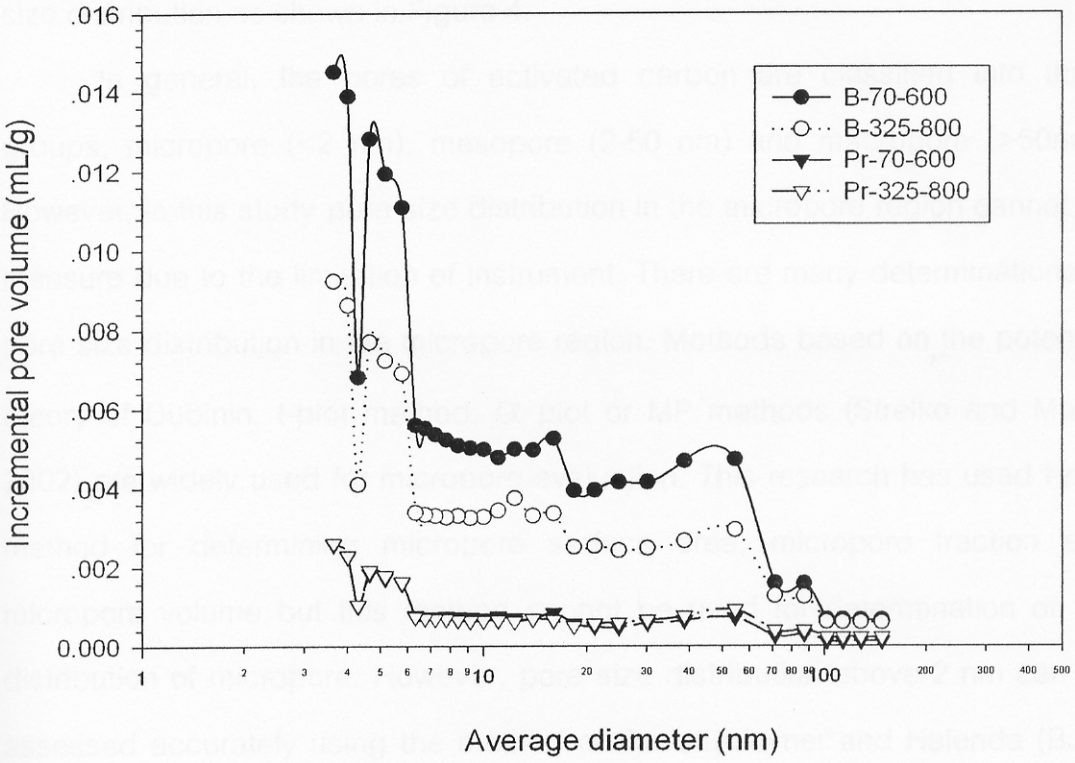

Figure 4 BJH pore size distribution of all activated carbons prepared from two agricultural wastes.

Although, adsorption tends to slightly decrease micropore volume of bagasse-based activated carbons compared with pericarp of rubber fruit based, it can be seen from Table 2 that Pr-70-600 and Pr-325-800 possess more micropore surface areas and percentages of micropore fraction (micropore surface area/ BET surface area) than the others. Both pericarp of rubber fruit based activated carbons show the large amounts of macropore due to they have micropore fraction around 70%. Noticeably, B-70-600 and B-325-800 have more BET surface areas than Pr-70-600 and Pr-325-800 but they

show less micropore fraction. This result is in good agreement with the pore size distribution as shown in Figure 4.

In general, the pores of activated carbon are classified into three groups, micropore (<2 nm), mesopore (2-50 nm) and macropore (>50nm). However, in this study pore size distribution in the micropore region cannot be measure due to the limitation of instrument. There are many determinations of pore size distribution in the micropore region. Methods based on the potential theory of Dubinin, t-plot method, α plot or MP methods (Strelko and Malik, 2002) are widely used for micropore evaluation. This research has used t-plot method for determining micropore surface area, micropore fraction and micropore volume but this method cannot be used for determination of the distribution of micropore. However, pore size distribution above 2 nm can be assessed accurately using the method of Barrett, Joyner and Halenda (BJH) model. (Barrett, et al., 1951)

The meso- and macropore nature (>2 nm) of all activated carbon is demonstrated in Figure 4. The pericarp of rubber fruit based activated carbons (which show similar shape of distribution) do not have significant mesopore and macropore. In contrast, B-70-600 possesses a significant amount mesopore with a maximum at 3 nm and 5 nm. Furthermore, it has more mesopores and macropores than the others entire distribution range. B-325-800 also shows the evidence of the presence of mesopores and macropore. The presence of mesopores and macropores of B-325-800 may affect to reduction of micropores while its BET surface area is highly remained.

Although, using different either chars particle sizes or activation temperatures, the method of activation seems to have no effect on the porous parameters significantly as can be seen from the results in Table 2 and Figure

4. Under many controversial issues, one expects that chars (or raw materials) with smaller particles sizes before activation should have more BET surface area. This study reveals clearly that it may not be significant from particle sizes of chars and temperatures in activation process.

It seems to be interested that types of raw materials affect porous characteristics. The bagasse based activated carbons possess both micropores and macropores. This contrast to pericarp of rubber fruit based activated carbons which possess large amounts of micropores. Therefore, the physical characteristics of raw materials seem to be important factor more than activation process for porous nature of activated carbons.

3.1.3 Fourier-transform infrared spectrophotometry (FT-IR)

Although numerous FT-IR spectroscopic studies have been conducted on various forms of carbon, the assignment of a specific wave number to a given functional group is not possible because the characteristic bands of various functional groups overlap and shift, depending on their molecular structures and environments (Fuente, et al., 2003). Nevertheless, a consensus in the assignment of band frequencies to different functional groups is possible to a certain extent.

The spectra of raw materials are shown in Figure 5 and 6. The strong band appears at about 3400 cm^{-1} is mainly assigned to O-H stretching vibrations of alcohol. The band observed at about 2900 cm^{-1} which is ascribed to symmetric and asymmetric C-H stretching vibrations in aliphatic CH, CH_2, and CH_3 groups are detected. The strong bands at about 1740 cm^{-1} is C=O stretching vibration in ketones. The band at about 1640 cm^{-1} is assigned to be C=O stretching vibration in quinones. The bands at about 1500

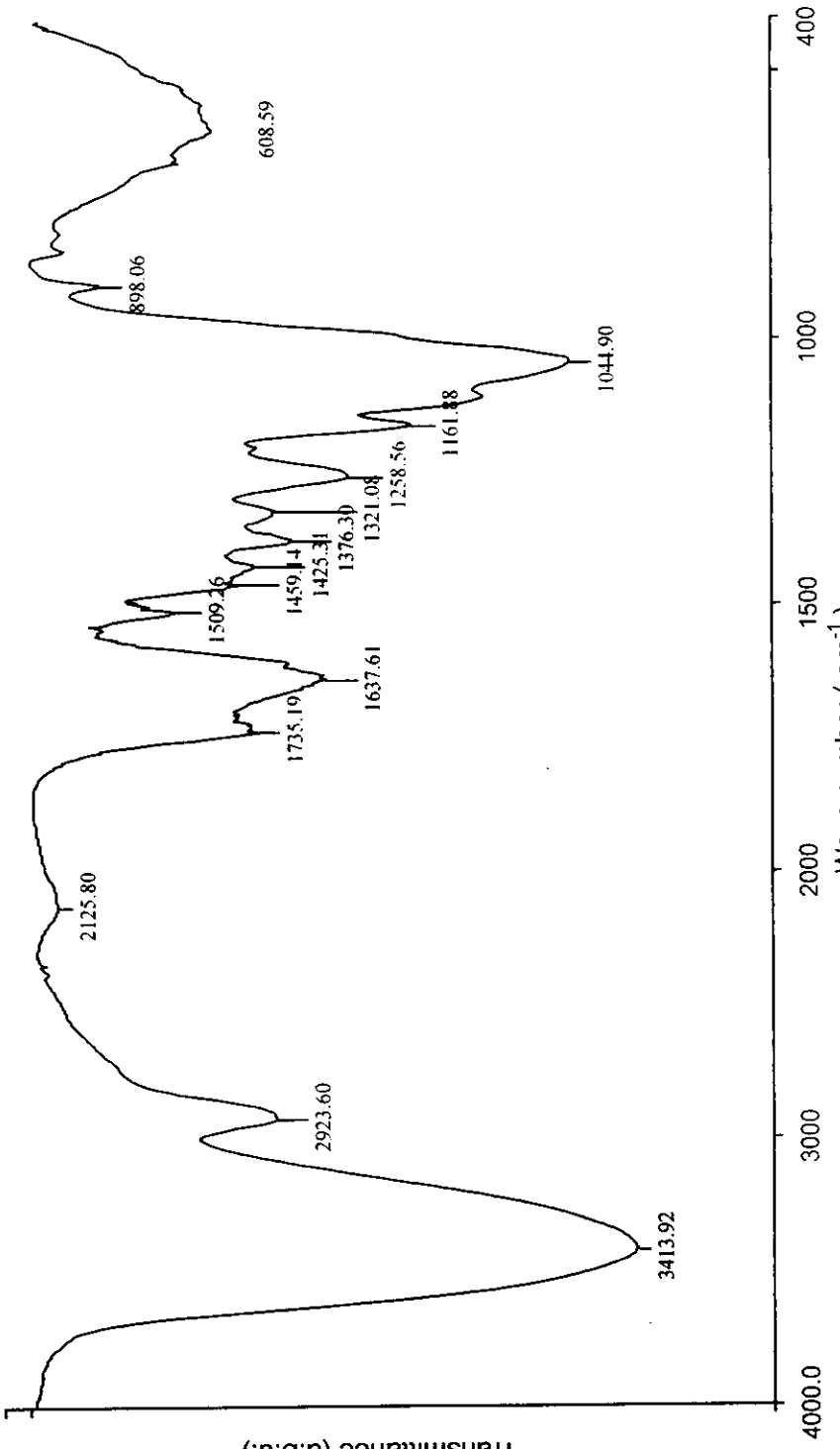

Figure 5 FT-IR spectrum of raw bagasse.

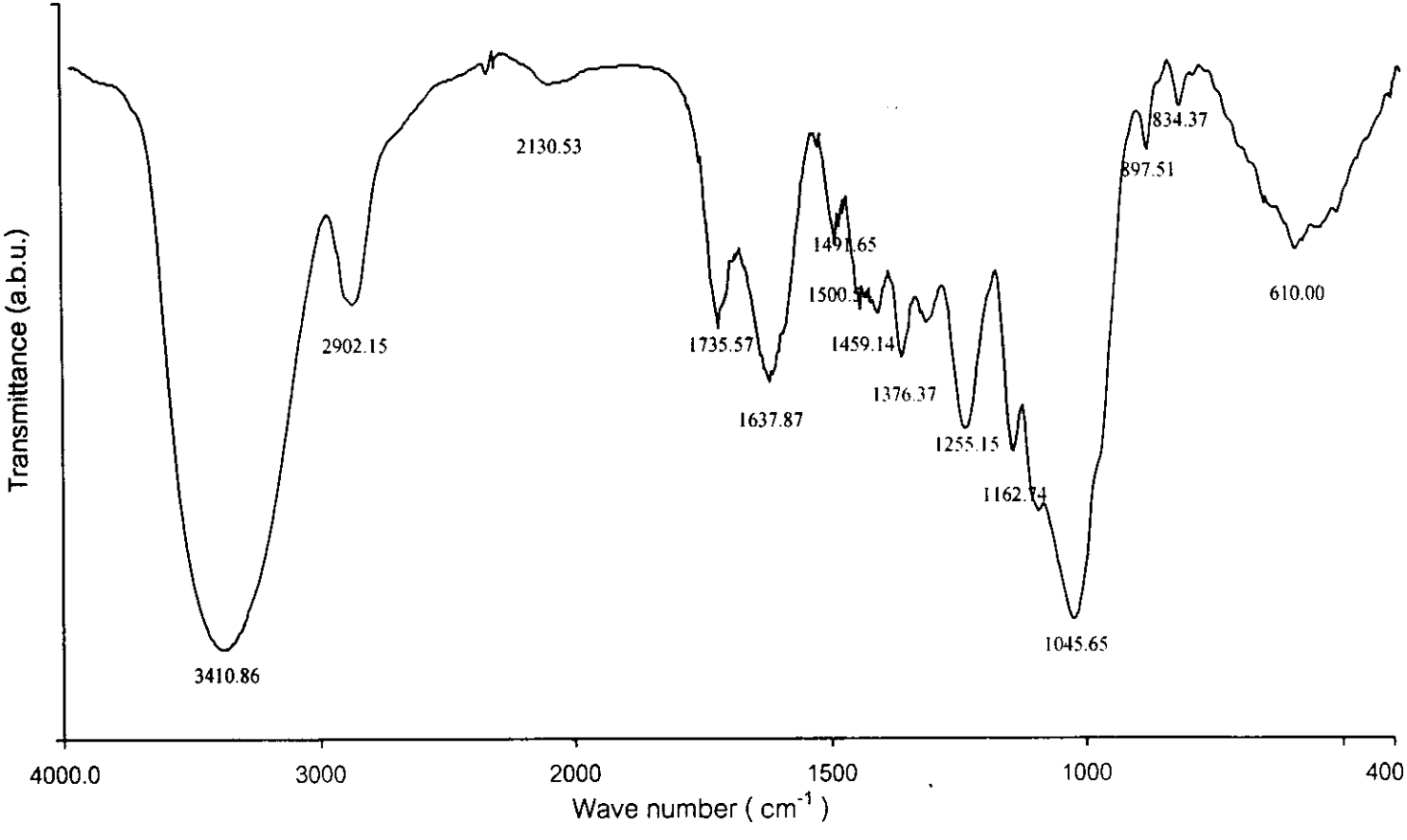

Figure 6 FT-IR spectrum of raw pericarp of rubber fruit.

cm^{-1} is C=C stretching vibration in aromatic rings. Many bands due to hydrogen, oxygen, sulphur and nitrogen functional groups are observed in the range 1400–400 cm^{-1} which are not mentioned herein except the strong band at about 1040 cm^{-1} can be attributed to C–O stretching vibrations. It is clear that appearance of the spectra of both raw materials due to chemical structures of cellulose, hemicellulose and lignin as shown in Figure 7.

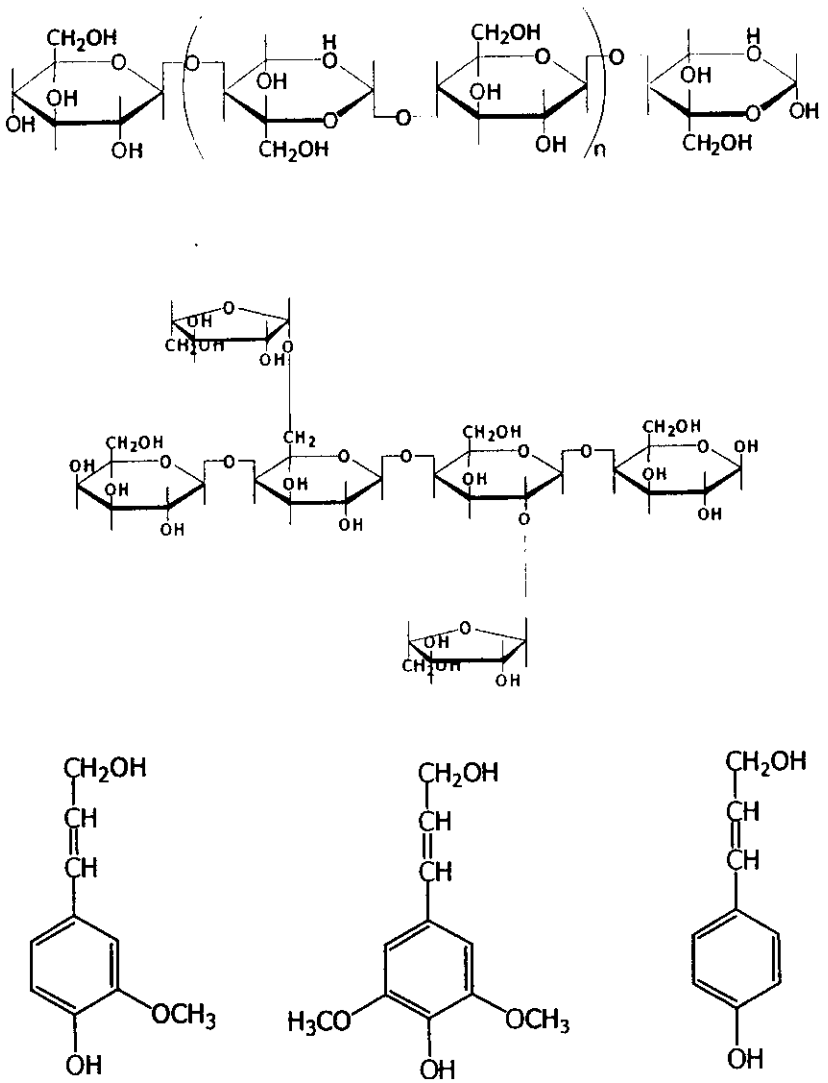

Figure 7 Chemical structures of cellulose, hemicellulose and lignin, respectively. (Jagtoyen and Derbyshire, 1998)

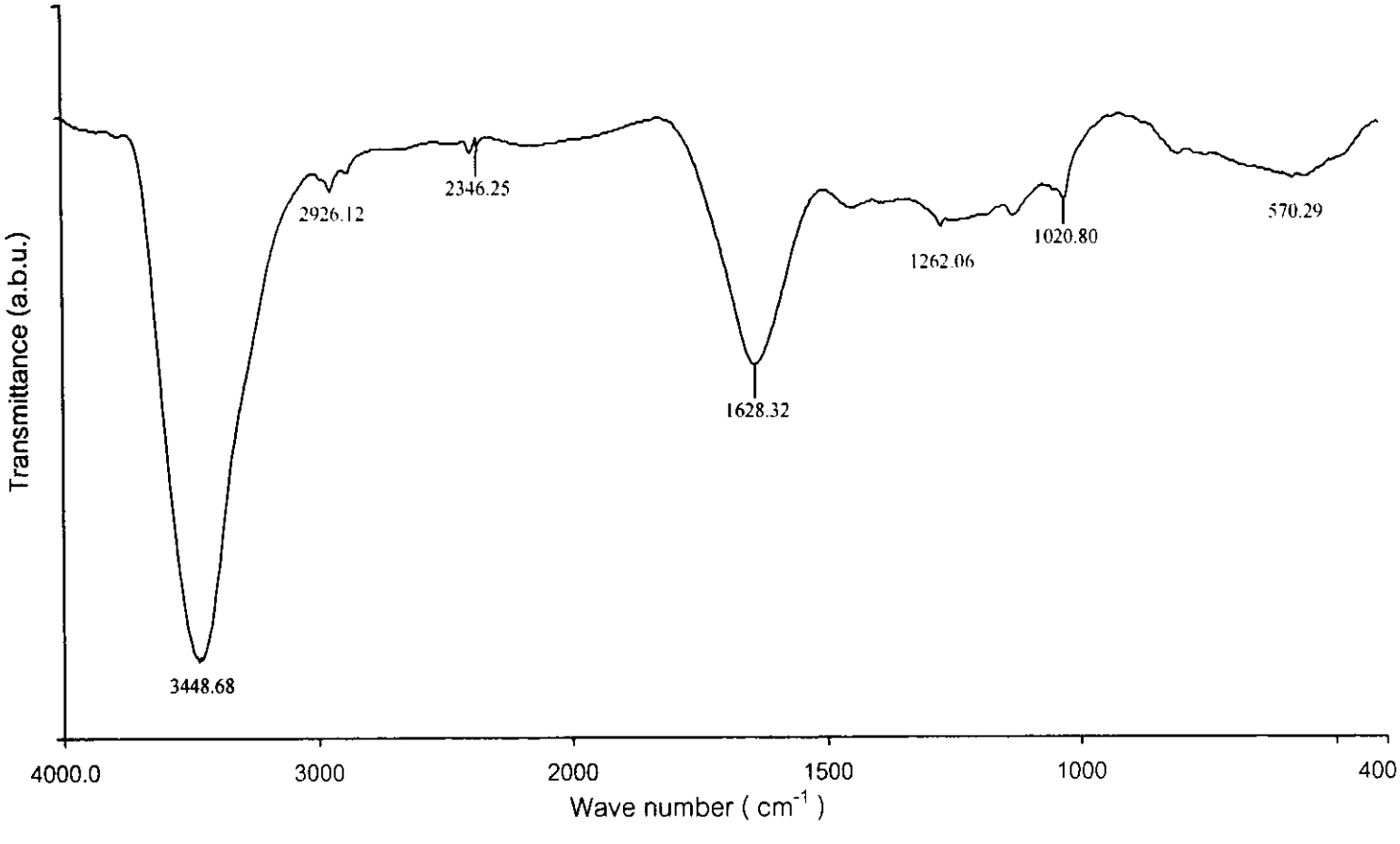

Figure 8 FT-IR spectrum of carbonized char of bagasse .

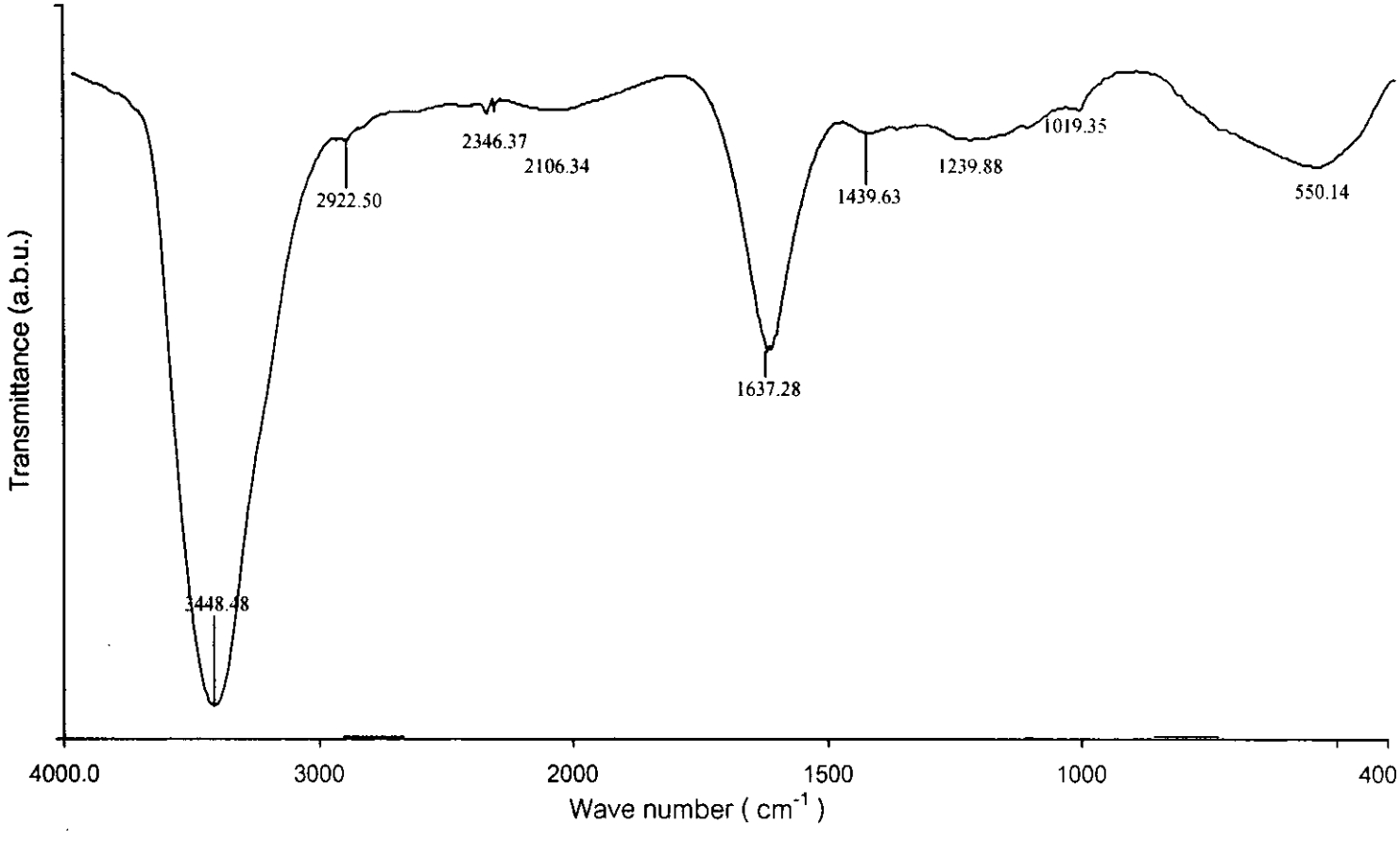

Figure 9 FT-IR spectrum of carbonized char of pericarp of rubber fruit .

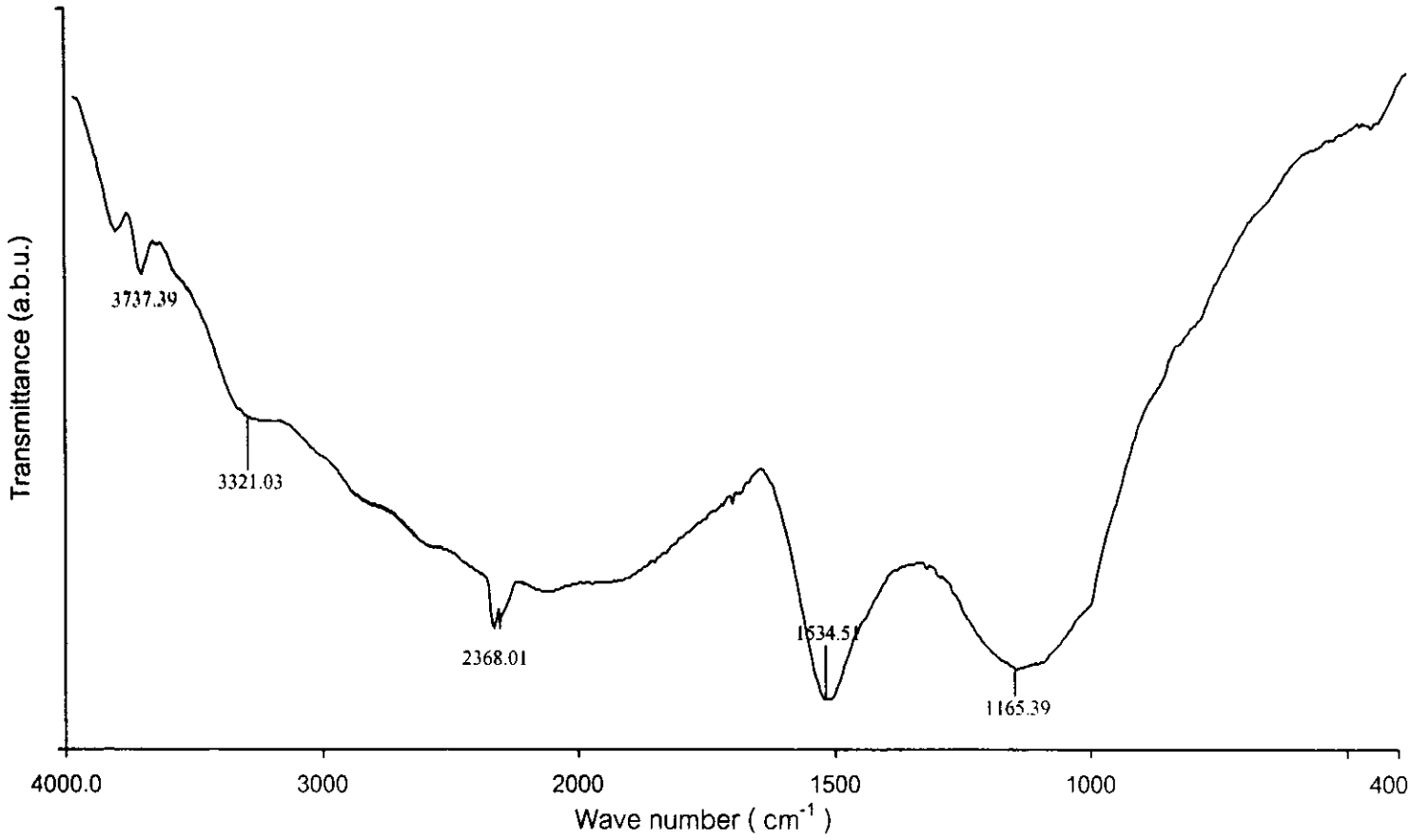

Figure 10 FT-IR spectrum of B-70-600.

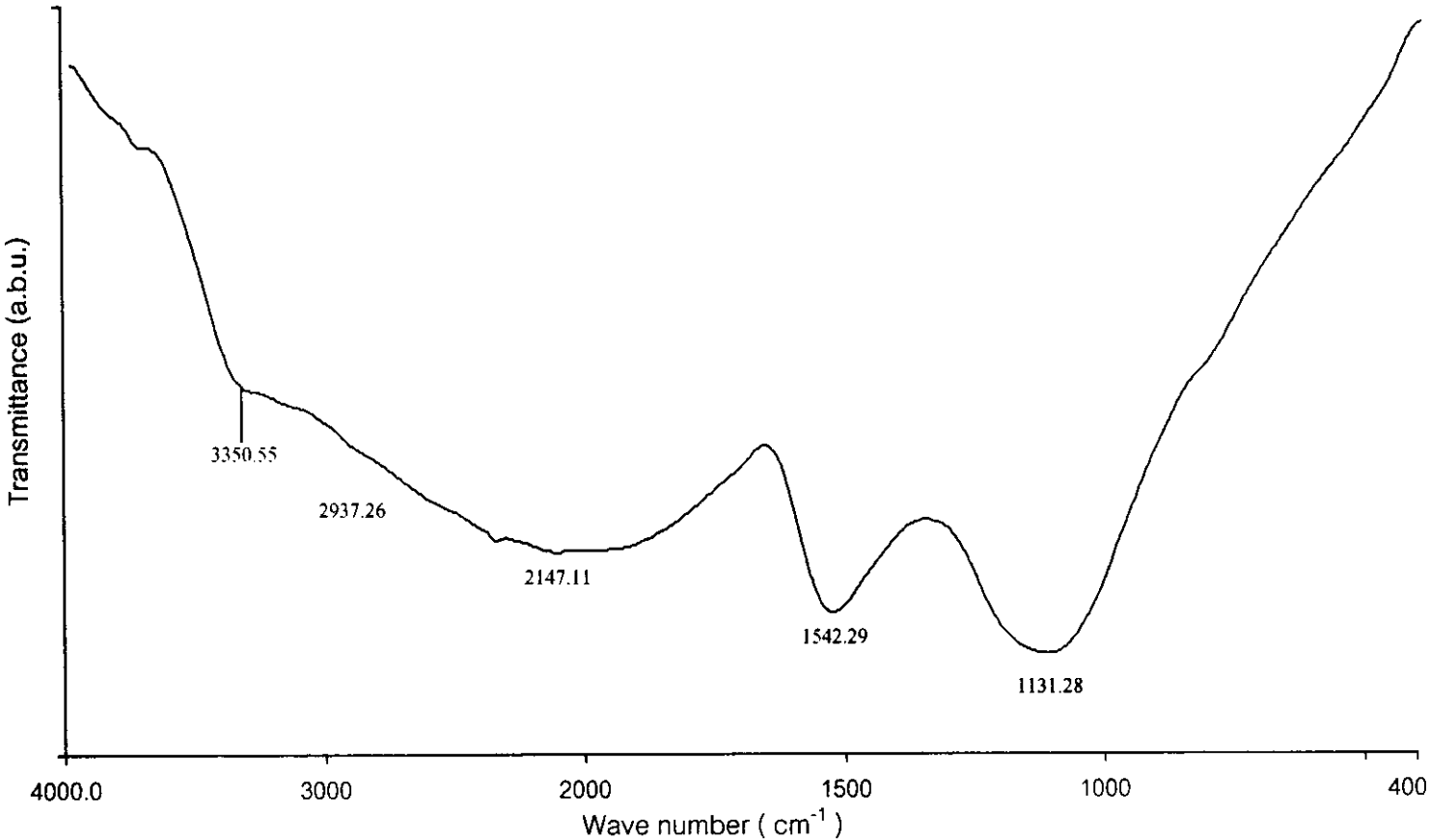

Figure 11 FT-IR spectrum of B-325-800.

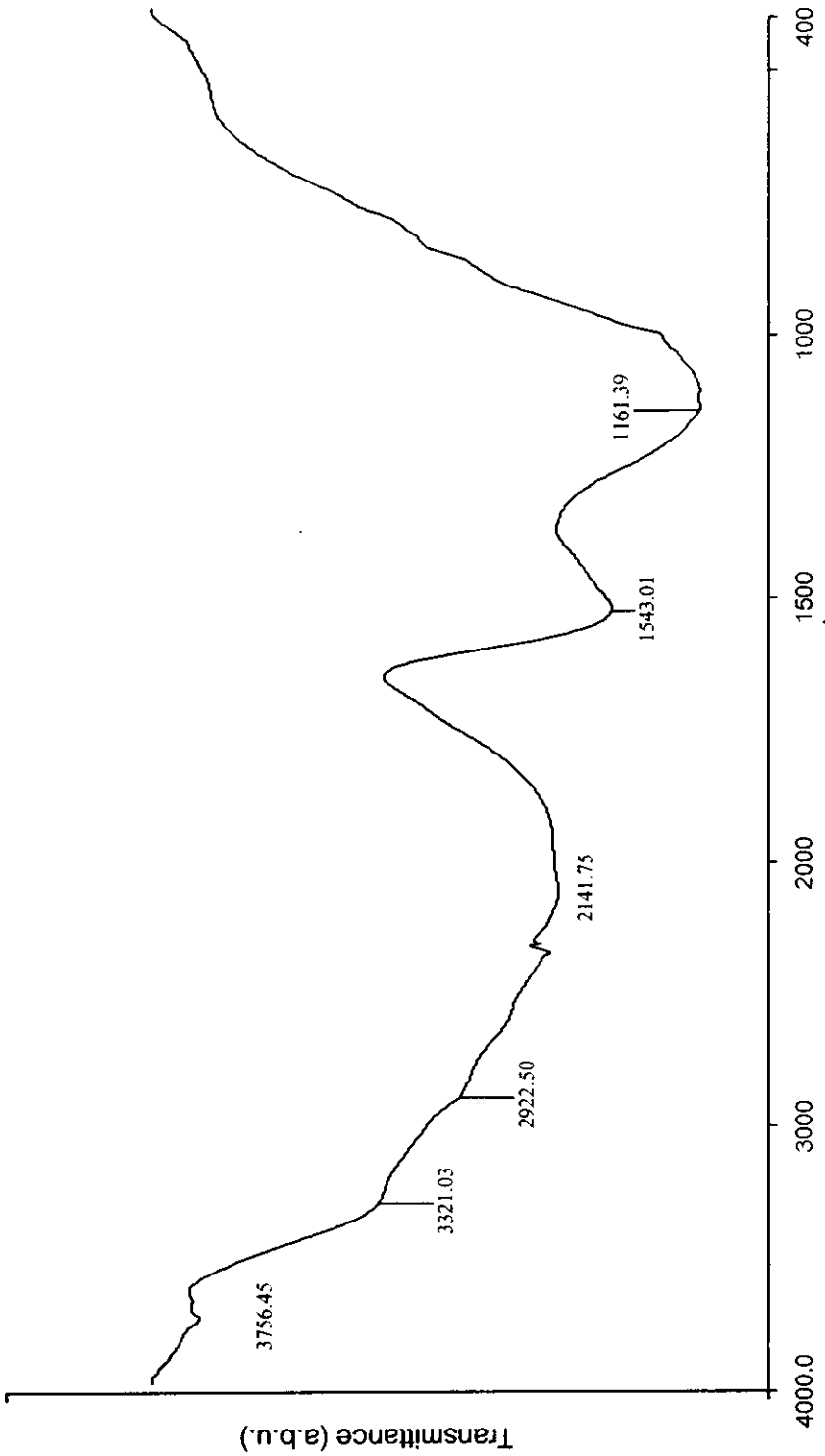

Figure 12 FT-IR spectrum of Pr-70-600.

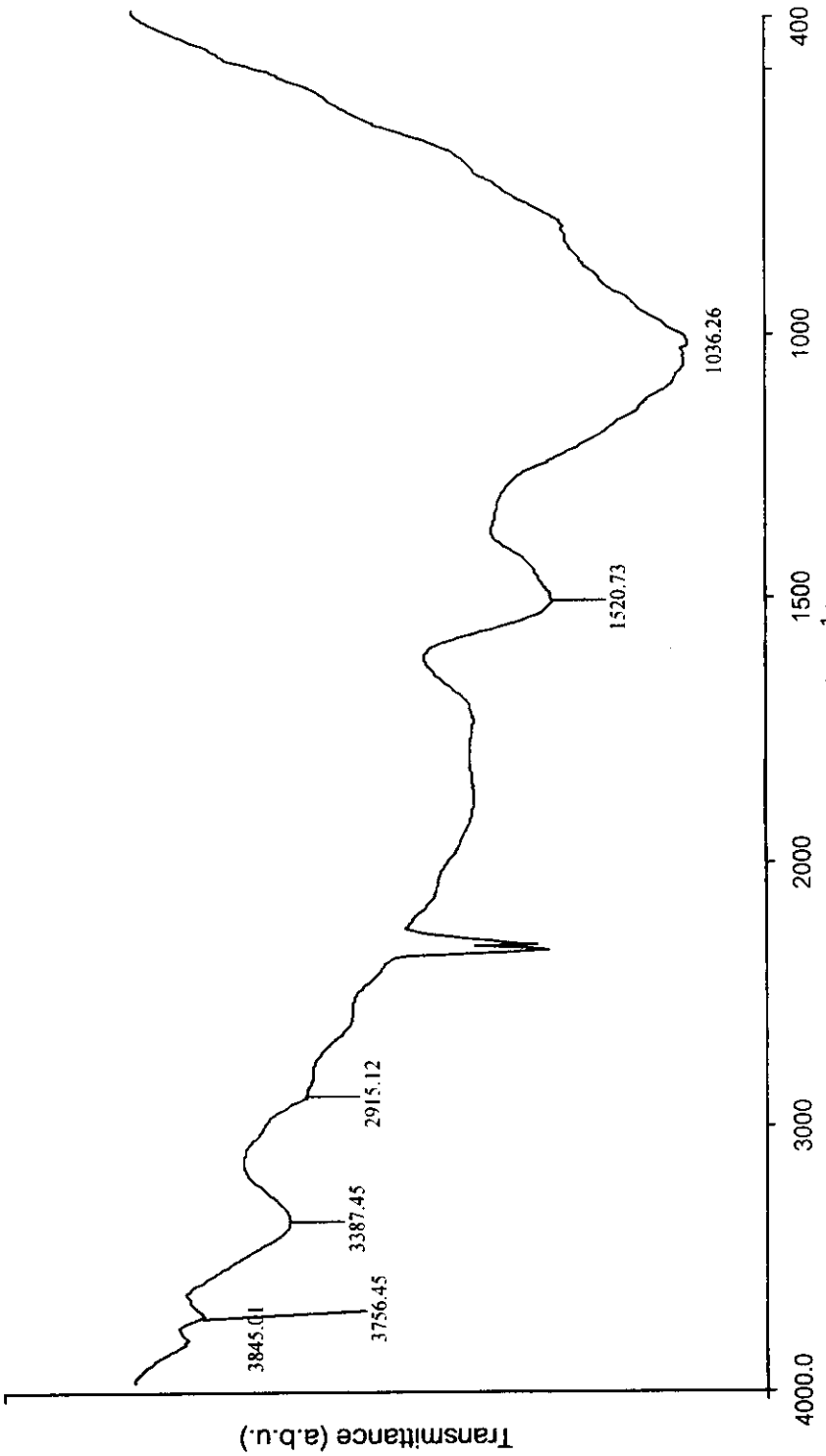

Figure 13 FT-IR spectrum of Pr-325-800.

After carbonization, both carbonized chars from different raw materials remain similar spectra (as shown in Figures 8 and 9) which many bands disappear when compare to those of raw materials. Both spectra show only two prominent bands at about 3400 cm^{-1} due to presence of O-H of alcohol and at about 1640 cm^{-1}which assigned to be C=O vibrations. The remaining of these bands may result from their thermal stabilities of those functional groups. Whereas, many bands in the range 1400-400 cm^{-1} are almost absent.

FT-IR spectra of activated carbon samples B-70-600, B-325-800, Pr-70-600 and Pr-325-800 are displayed in Figures 10, 11, 12 and 13, respectively. All activated carbon samples show very similar spectra. The band appears at about 3400 cm^{-1}, assigned to O-H stretching vibration is remained but relatively low intensity compare to raw materials and chars. While the bands at 1640 cm^{-1} are absent. There is a new strong band at about 1540 cm^{-1} which can be assigned to C=C aromatic ring vibration augmented by the presence of the oxygen double bond conjugated with the carbon basal planes. This band is the characteristic peak of carbon materials (Fuente, et al., 2003). Furthermore, the characteristic band due to C–O stretching vibrations is observed in the range 1300 – 900 cm^{-1}. It is difficult to assign each simple motion of specific functional groups or chemical bonds in this region. The band at about 1200 – 1100 cm^{-1} in the FT-IR spectra of all activated carbons studied can be assigned to C–O stretching vibrations in ether structures or sometime assigned to be the etheric (symmetrical stretching vibration) epioxide and O-H bending modes (Buczek, et al.,1999).

As mentioned above, although using different raw materials and activation process, all activated carbon samples still have similar spectra. It does not mean chemical nature of activated carbons will not be different.

Unfortunately, FT-IR can be used only to characterize functional groups on the carbon surfaces qualitatively. Quantitative analysis by using this method is difficult to distinguish the nature of carbons. It is necessary to employ other methods for clear chemical characterizations. However, FT-IR which used in this study can distinguish the structural change from the raw materials to chars and chars to activated carbons clearly by comparison of different bands in each steps. As a results, it can be seen that creation of C=C band as the characteristic bands does not appear only carbonized steps (300 and 400 ^{o}C). While using $ZnCl_2$ as the activated reagent and further activation at higher temperatures (600 and 800 ^{o}C) can create C=C bonds in activated carbons as may result from decomposition of other functional groups and shrinkage of other C-C, C-H, C-O or C-N bonds to C=C bonds.

3.1.4 Point of zero charge measurements (pH_{pzc})

The graphs of final pH versus initial pH obtained by using pH drift method (Jia, et al., 2002) for all activated carbon samples are shown in Figure 14. The results show that all of activated carbons have acidic surface characteristics as pH_{pzc} values have been found that less slightly than 7 (The graphs of final versus initial pH are used to determine the points at which initial pH and final pH values were equal. This is taken as the pH_{pzc} of the activated carbon). Noticeably, activated carbons which ground to 70 mesh and activated at 600 ^{o}C (B-70-600 and Pr-70-600) are more acidic ($pH_{pzc} \approx 5$) than those ground at 325 mesh and activated at 800 ^{o}C ($pH_{pzc} \approx 5.7$).

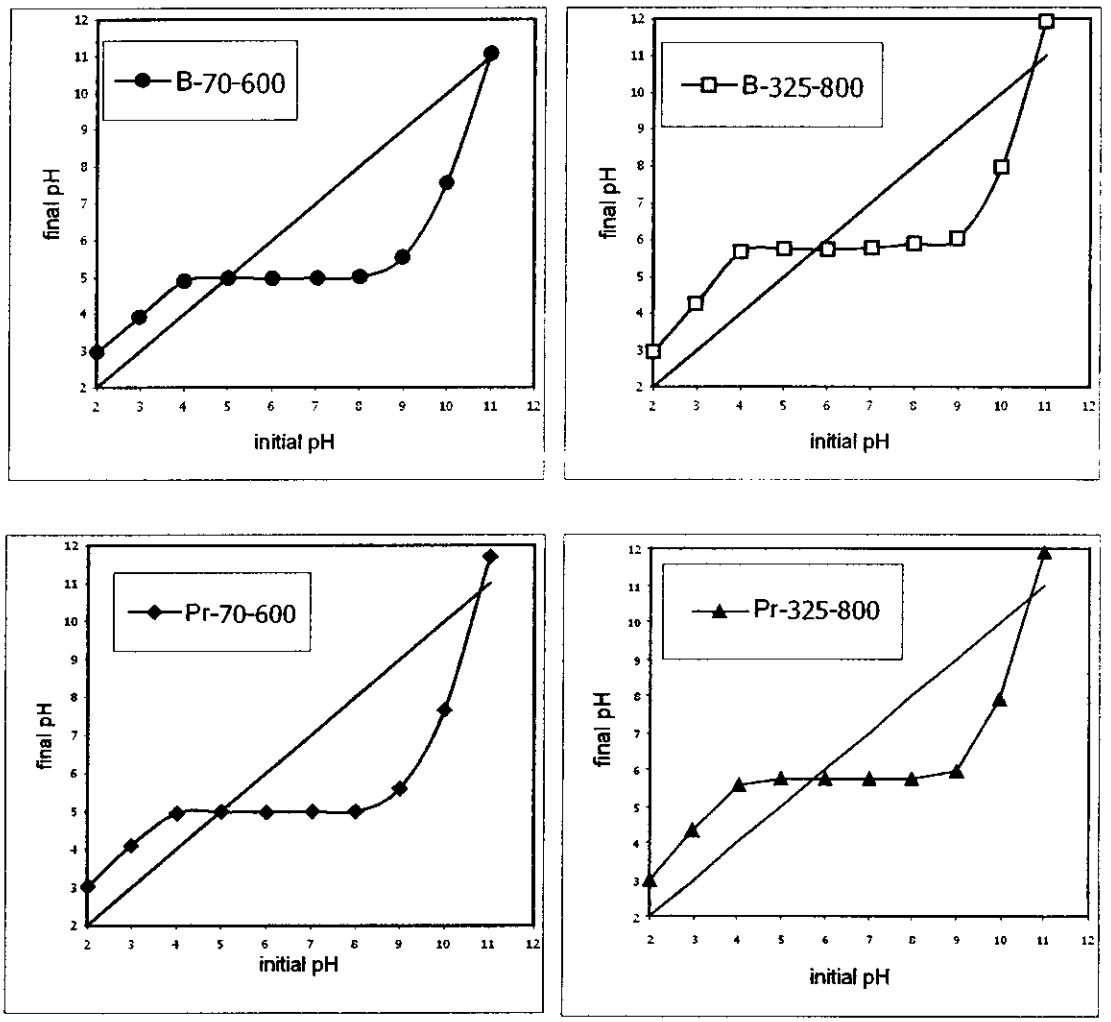

Figure 14 Graph of final pH versus initial pH obtained by using the pH drift method.

It shows the amphoteric character of surface oxides S-CO_2, where S represents the activated carbon surface (Kadirvalu, et al., 2000).

For pH < pH_{pzc}, the dominant reaction is:

$$S\text{-}CO_2 + 2H_2O \leftrightarrow S\text{-}C(OH^+)_2 + 2OH^-.$$

The release of hydroxyl ions induces an increase of pH and a protonated surface of activated carbon.

For pH > pH_{pzc}, the following reaction takes place:

$$S\text{-}CO_2 + 2H_2O \leftrightarrow S\text{-}C(O^-)_2 + 2H_3O^+.$$

The actvated carbon surface is deprotonated and the release of protons induces a decrease in pH.

The pH and acid–base values of the activated carbons give a good indication of the surface oxygen complexes and the electrical surface changes undergone by them. These surface changes arise from the interaction between the carbon surface and the aqueous solution. The complexes on the carbon surfaces are generally classified as acidic, basic, and neutral groups. Meanwhile, the surface acidity is an important property of hydrous solids, which relates to the extent of interfacial reactions, such as the adsorption of alkaline metals. Upon hydration the solid surface develops hydroxyl groups which behave as Bronsted acids (Park and Jang, 2002), The distribution diagram of surface hydroxyl groups as a function of pH is constructed, such as that shown in Figure 15 (Park and Jang, 2002).

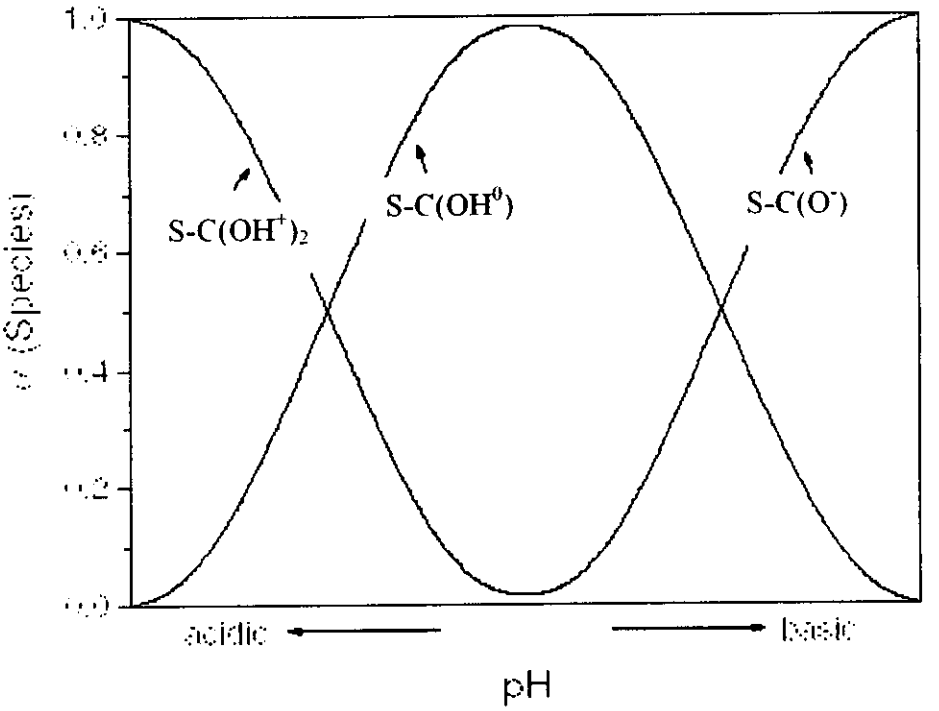

Figure 15 Speciation diagram of surface functional groups on activated carbons (Park and Jang, 2002).

3.2 Adsorption studies

3.2.1 Adsorbate metal ions solution

Knowledge of the speciation diagram of the adsorbate is necessary for an understanding of the adsorption mechanism.

Firstly, it should be pointed out that the solubility of the metal halides used in this study in 100 g of water is 110.6 g of $CdCl_2$ at 291 K and 1.08 g of $PbCl_2$ at 298 K and that, consequently, in the 10 to 200 ppm concentration range the metal halides completely dissolved in water (Burgess, 1978).

Secondly, in aqueous solution, it should be considered the formation of metal ions. For $CdCl_2$ it is usually assumed that undissociated molecules are

present in considerable concentration in addition to complex ions, $[CdCl_3]^-$. The following equillibria have been proposed (Remy, 1956):

$$Cd^{2+} + 3Cl^- = CdCl_2 + Cl^- = [CdCl_3]^-$$

In the absence of excess Cl^- ions, however, the main dissociation equilibrium for $CdCl_2$ may be

$$CdCl_2 = Cd^{2+} + 2Cl^-$$

The saturated $PbCl_2$ solution has an apparent content of 6% of undissociated salt at 25°C; about half of the remaining lead chloride undergoes primary dissociation (Remy, 1956):

$$PbCl_2 = PbCl^+ + Cl^-$$

and half undergoes secondary dissociation:

$$PbCl_2 = Pb^{2+} + 2Cl^-$$

The Cd^{2+} and Pb^{2+} ions in aqueous solution may suffer solvation, hydrolysis and polymerization (Burgess, 1978), the processes involved for dipositive ions being, in turn, the following:

$$M^{2+} + nH_2O = M(H_2O)_n^{2+}$$

$$M(H_2O)_n^{2+} = M(H_2O)_{n-1}(OH)^+ + H^+$$

$$nM^{2+} + mH_2O = Mn(OH)_m^{(2n-m)+} + mH^+$$

According to the literature review (Baes and Mesmer, 1976), Cd^{2+} and Pb^{2+} can form several hydrolysis products, which exist under widely varying conditions. For Pb^{2+}, a number of polynuclear species such as $Pb_2(OH)^{3+}$, $Pb_3(OH)_4^{2+}$, etc., have also been reported. In diluted solutions, however, the formation of Cd^{2+} and Pb^{2+} hydrolysis products occurs at pH above 6, especially for Pb^{2+} (Baes and Mesmer, 1976). It is reasonable to conclude that metal hydroxide species are not important in relation to equilibrium with the surface at the metal ion concentrations and pH range (1-6) used in this study. Furthermore, this shows that Cd^{2+} and Pb^{2+} in the adsorptive solution are likely found as free ions in equilibrium with solvated species. The hydration numbers for metal ions have been determined by a variety of physical techniques. The proposed values for Cd^{2+} and Pb^{2+} range widely between 12 and 4.6 and between 8 and 4, respectively (Burgess, 1978).

3.2.2 pH effect on adsorption of cadmium and lead ions on activated carbons

The effect of solution pH values on the adsorption of cadmium and lead ions on all of the activated carbons are shown in Figure 16 (a) and (b), respectively. Both cadmium and lead ions display a general trend of increased adsorption on all the activated carbons with the increase of solution pH values. At pH below 2, almost no adsorption of cadmium and lead ions take place. For higher pH from 2, the adsorption amount of both ions on all of the samples increased consistently with the increase of solution pH values. It seems to indicate that for all samples at low pH (< 2) electrostatic repulsion between metal ions and the positively charged surface of activated carbons takes place. Furthermore, at low pH there is competition for the surface sites of activated carbon between protonation (H^+ adsorption on the carbon surface)

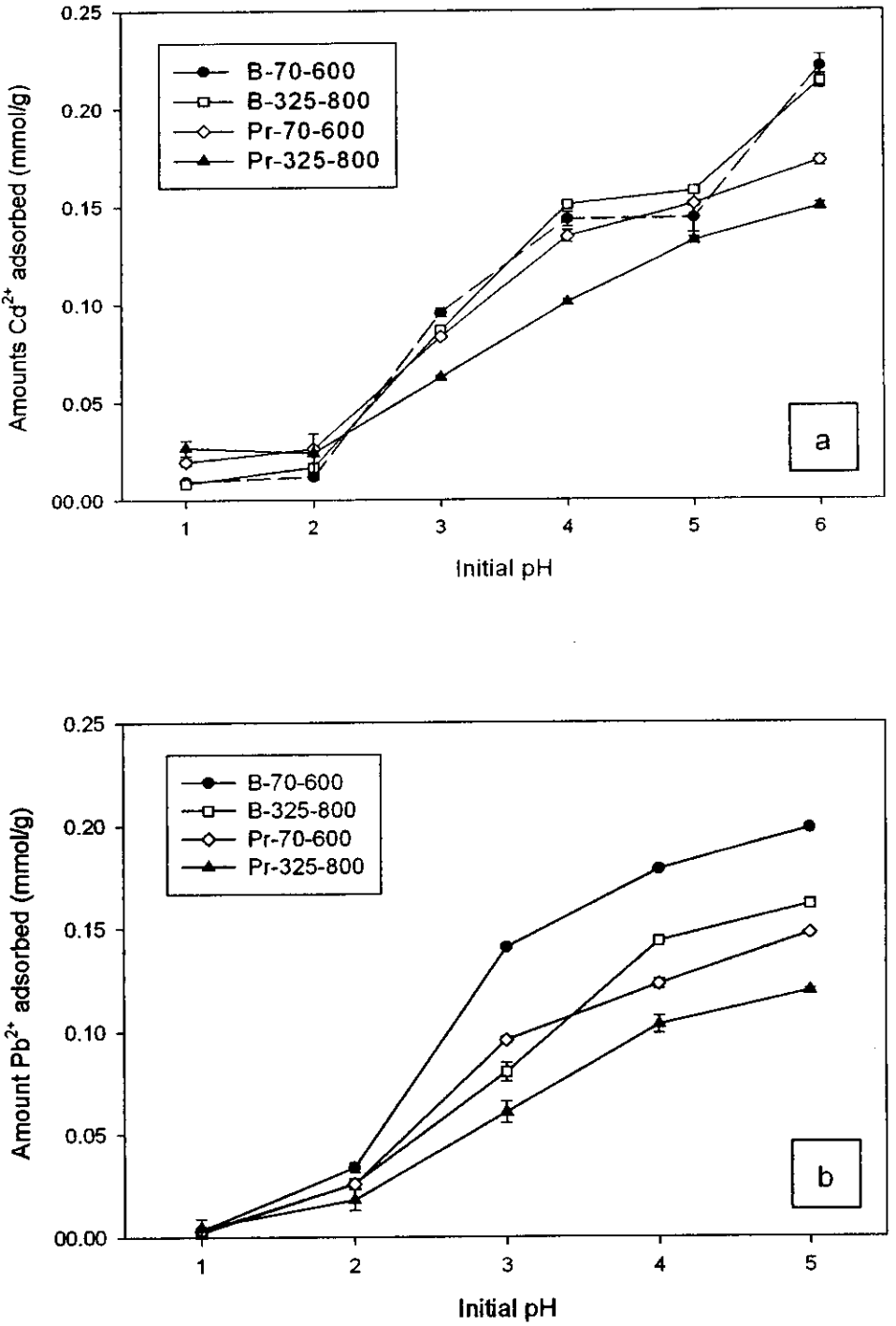

Figure 16 Adsorption of Cd^{2+} (a) and Pb^{2+} (b) by the obtained activated carbon samples as a function of initial pH of solution: (concentration = 80 ppm).

and adsorption of metal ions. Since the pH_{pzc} of all samples are positive at pH < 6 (pH_{pzc} = 5 for B-70-600 and Pr-70-600 and pH_{pzc} = 5.7 for B-325-800 and Pr-325-800 as shown above in Figure 14), the electrostatic interactions between the carbon and metal ions to be adsorbed are electrically repulsive under the pH values studied as Cd^{2+} and Pb^{2+} are the major species in the solutions at pH below 6 and 5, respectively. It may be possible that when pH is below 2, the strong electrical repulsion prevented the metal ions from contacting the activated carbon surfaces, resulting in almost no adsorption of both ions. With the increase of solution pH values, the electrical repulsion force become weaker and the metal ions may be transported to the surface of the activated carbons and become to attach on the surface due to the action of other factors such as less competitive from protonation as mentioned above.

3.2.3 Adsorption isotherm studies of cadmium and lead ions on activated carbons

The adsorption kinetics of metal ions adsorption onto the obtained activated carbons were studied in order to assess the time required for equilibrium to be achieved. In almost adsorption kinetics studies, the results showed that equilibrium was achieved within around 3 h. However, the solutions were left for 6 h to ensure complete equilibration.

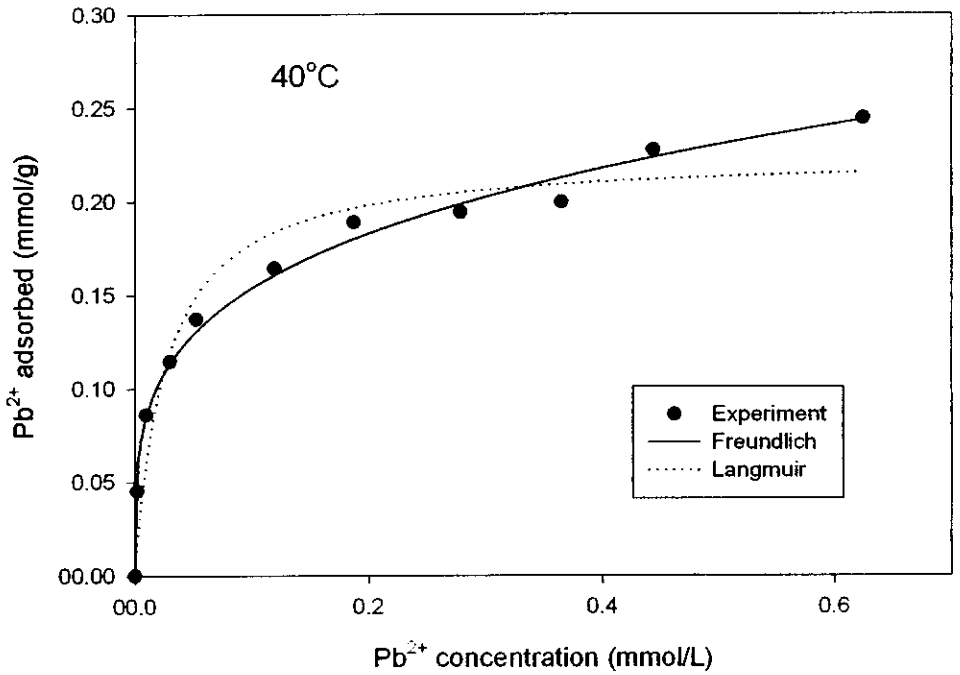

Figure 17 Adsorption isotherm of Pb^{2+} on B-70-600 at temp = 40°C, pH = 5.

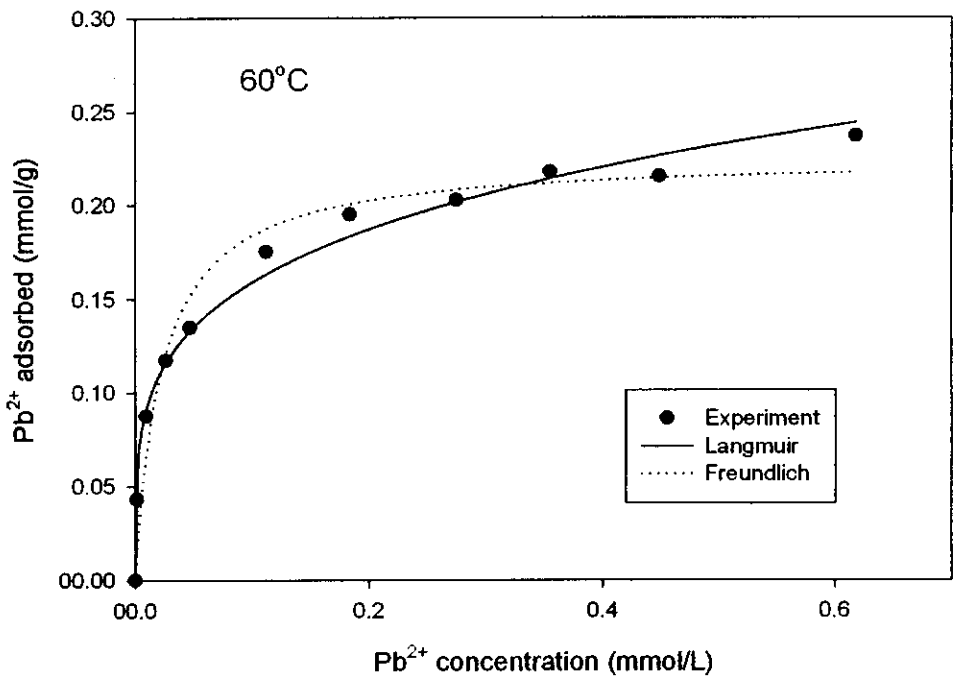

Figure 18 Adsorption isotherm of Pb^{2+} on B-70-600 at temp = 60°C, pH = 5.

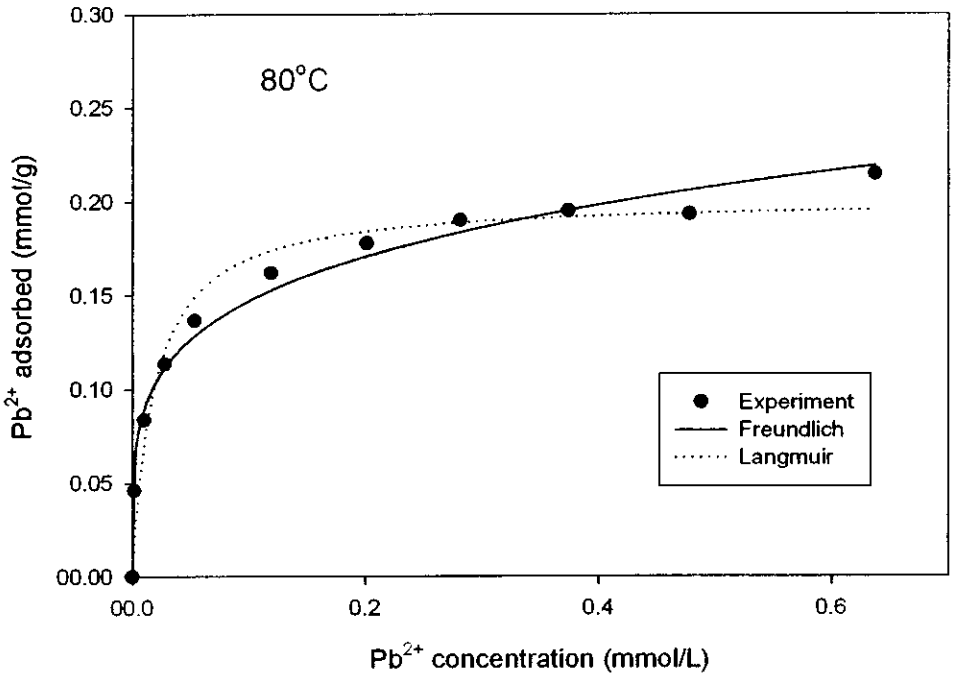

Figure 19 Adsorption isotherm of Pb^{2+} on B-70-600 at temp = 80°C, pH = 5.

Table 3 Parameter values of the Langmuir and Freundlich equations fitted to the experiment of Pb^{2+} adsorption on B-70-600 at different temperatures.

temp	Langmuir			Freundlich		
(°C)	b	Q_m	r^2	K_F	n	r^2
40	37.955	0.2242	0.9413	0.274	0.2513	0.992
60	44.506	0.2251	0.9625	0.2732	0.2352	0.9879
80	52.989	0.2013	0.9613	0.2415	0.2161	0.9864

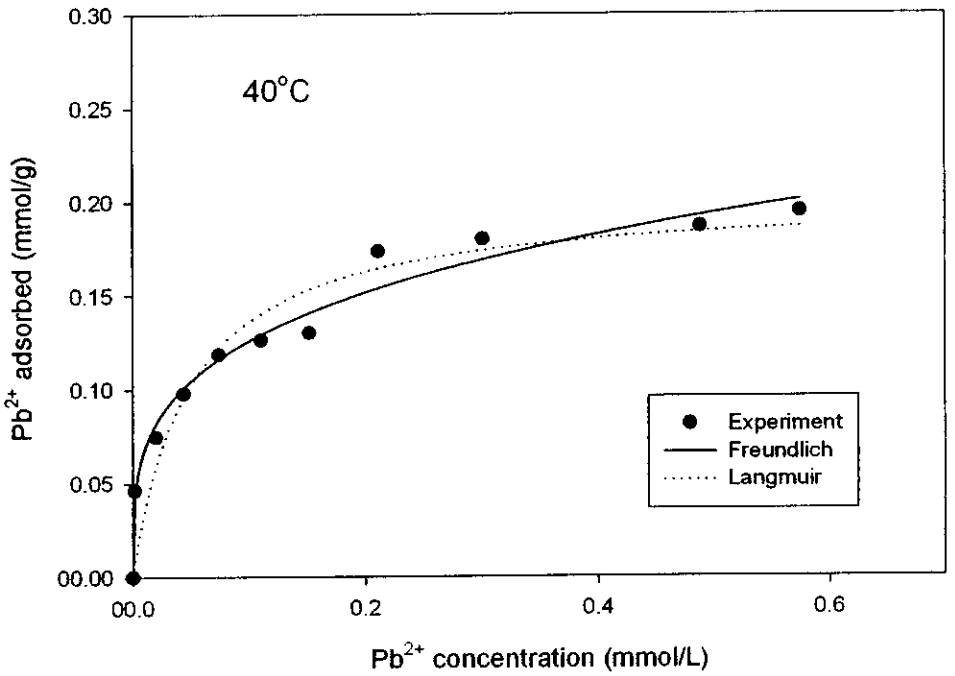

Figure 20 Adsorption isotherm of Pb^{2+} on B-325-800 at temp = 40°C, pH = 5.

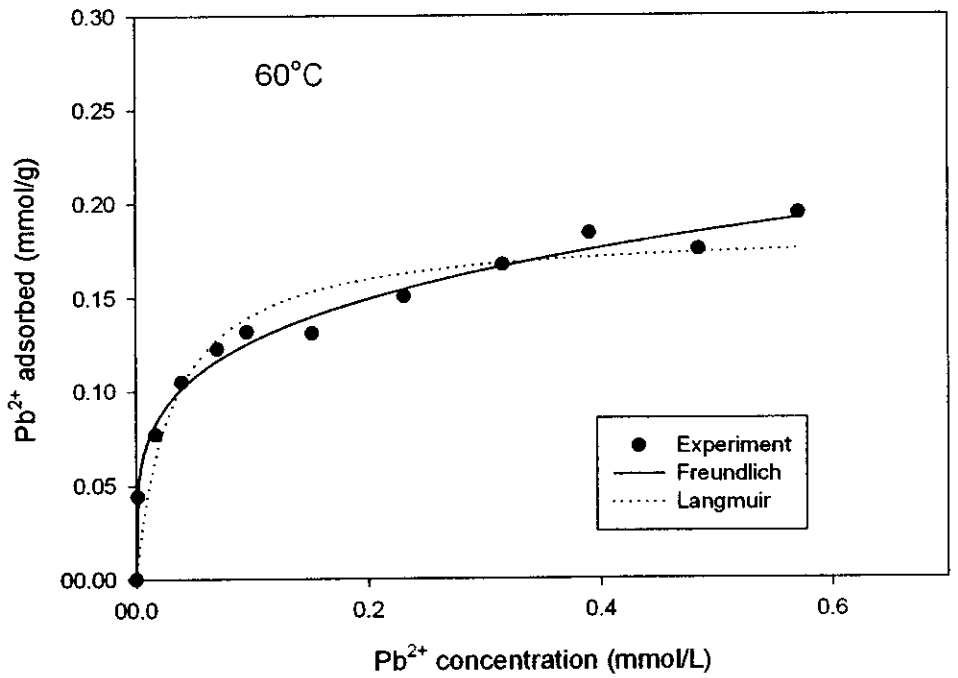

Figure 21 Adsorption isotherm of Pb^{2+} on B-325-800 at temp = 60°C, pH = 5.

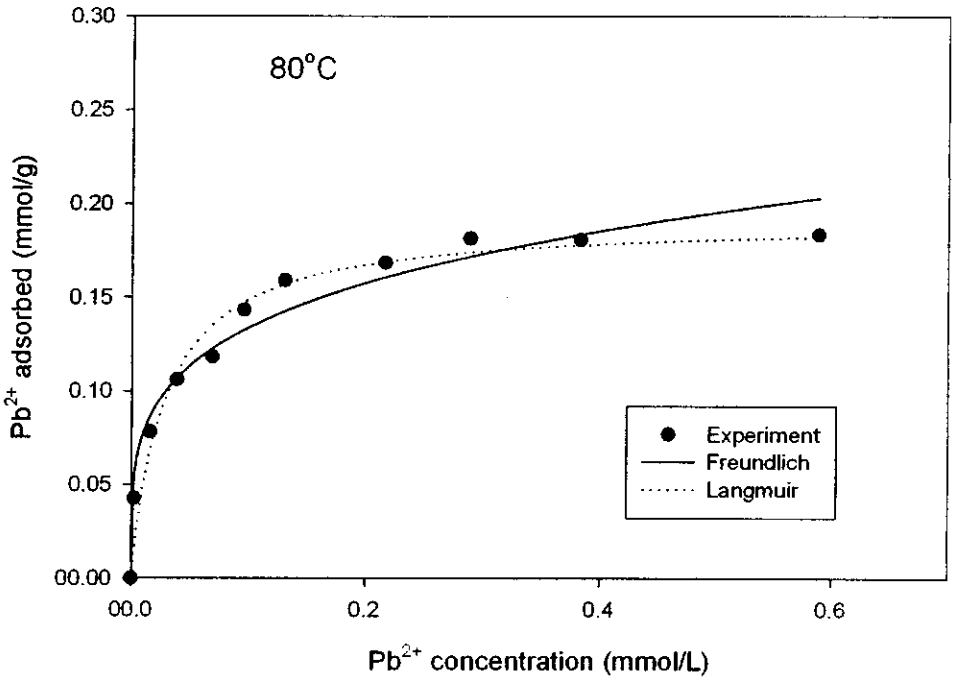

Figure 22 Adsorption isotherm of Pb^{2+} on B-325-800 at temp = 80°C, pH = 5.

Table 4 Parameter values of the Langmuir and Freundlich equations fitted to the experiment of Pb^{2+} adsorption on B-325-800 at different temperatures.

temp	Langmuir			Freundlich		
(°C)	b	Q_m	r^2	K_F	n	r^2
40	20.526	0.2021	0.9306	0.2331	0.2677	0.9797
60	31.62	0.185	0.929	0.2191	0.2385	0.9896
80	35.125	0.1909	0.9665	0.2298	0.2349	0.9688

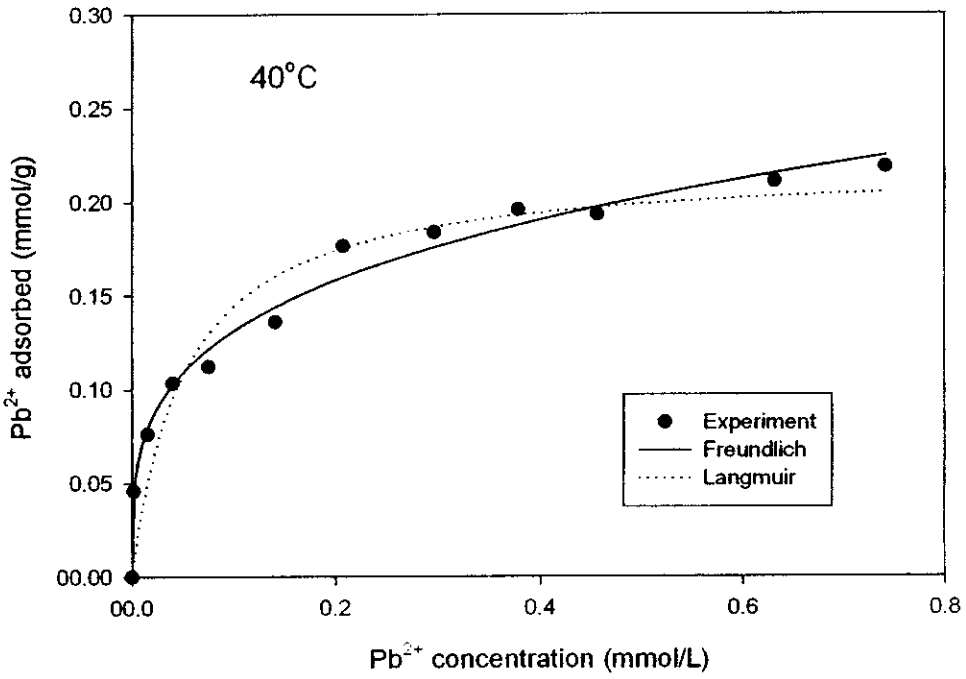

Figure 23 Adsorption isotherm of Pb^{2+} on Pr-70-600 at temp = 40°C, pH = 5.

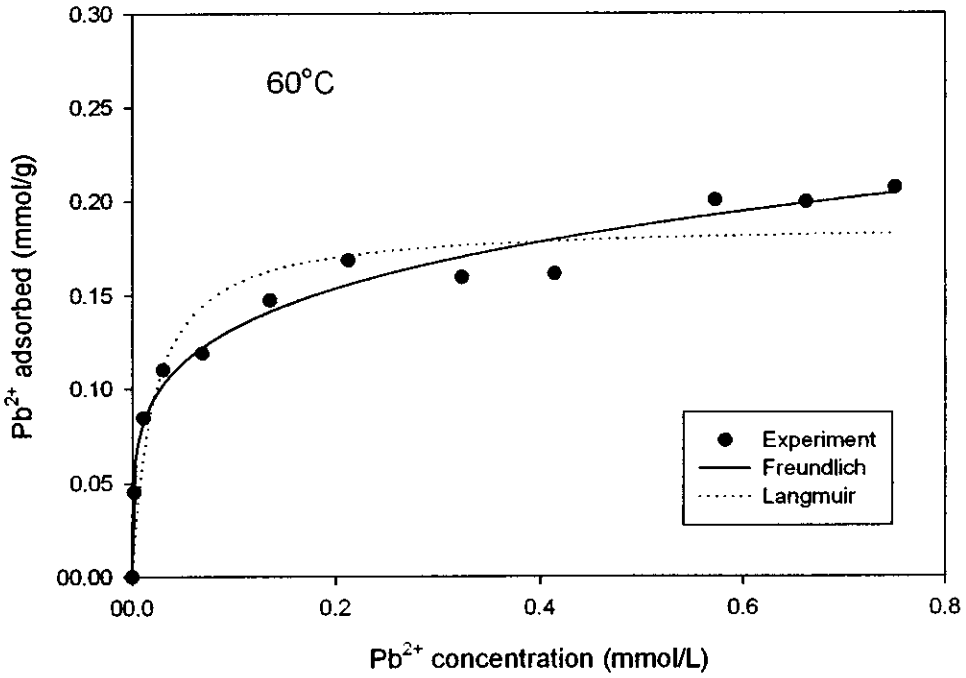

Figure 24 Adsorption isotherm of Pb^{2+} on Pr-70-600 at temp = 60°C, pH = 5.

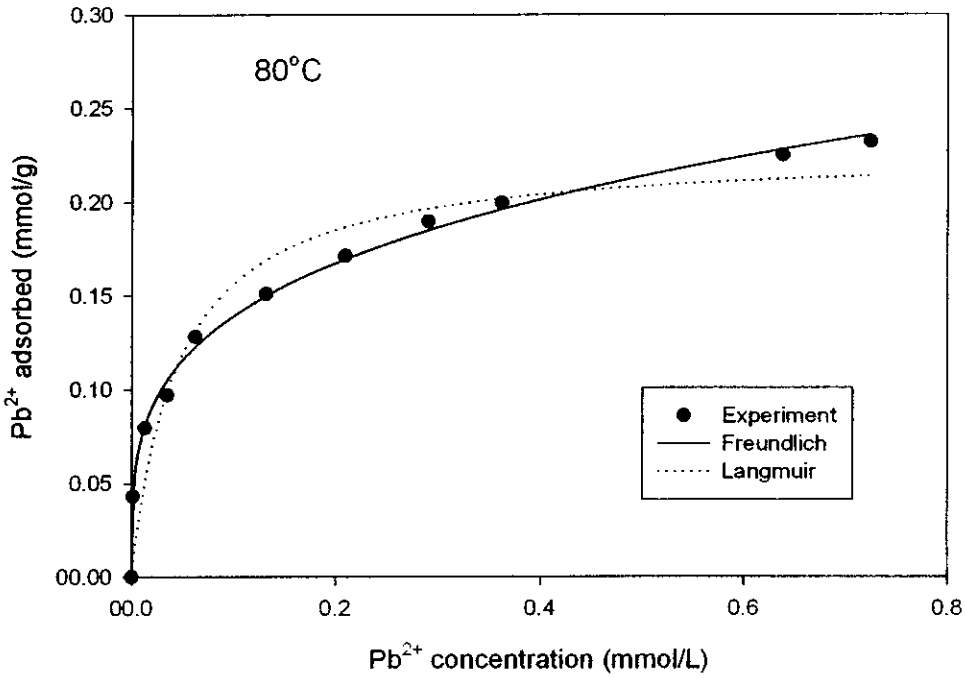

Figure 25 Adsorption isotherm of Pb^{2+} on Pr-70-600 at temp = 80°C, pH = 5.

Table 5 Parameter values of the Langmuir and Freundlich equations fitted to the experiment of Pb^{2+} adsorption on Pr-70-600 at different temperatures.

temp	Langmuir			Freundlich		
(°C)	b	Q_m	r^2	K_F	n	r^2
40	19.295	0.2192	0.9382	0.2432	0.2677	0.9881
60	48.89	0.1875	0.9107	0.2169	0.2143	0.9799
80	21.997	0.2272	0.9425	0.257	0.2661	0.9972

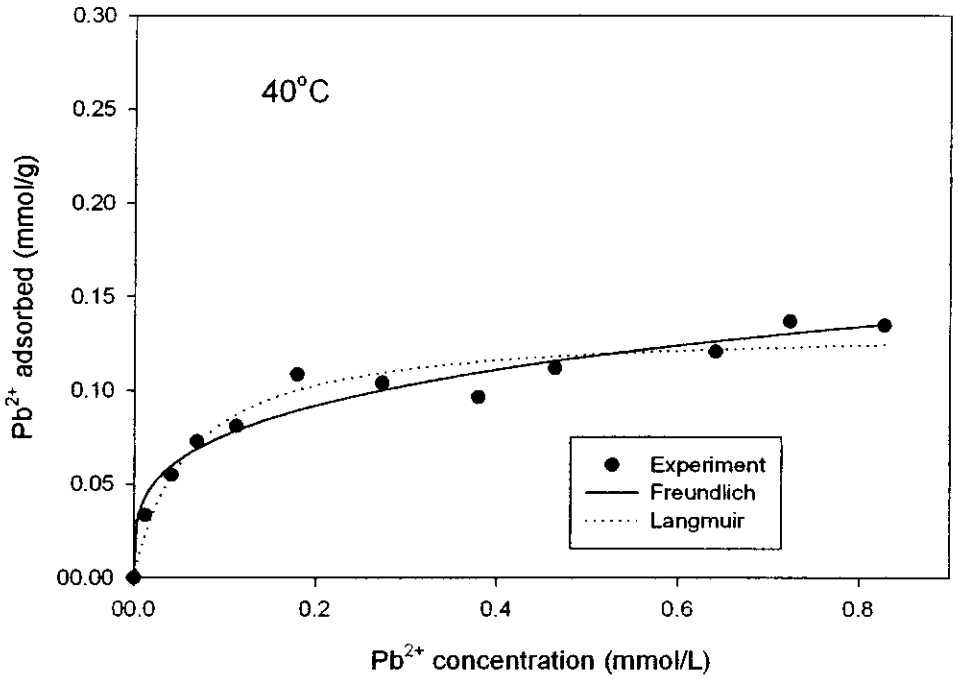

Figure 26 Adsorption isotherm of Pb^{2+} on Pr-325-800 at temp = 40°C, pH = 5.

Table 6 Parameter values of the Langmuir and Freundlich equations fitted to the experiment of Pb^{2+} adsorption on Pr-325-800 at temp = 40°C.

temp	Langmuir			Freundlich		
(°C)	b	Q_m	r^2	K_F	n	r^2
40	16.989	0.1329	0.95	0.1422	0.271	0.9593

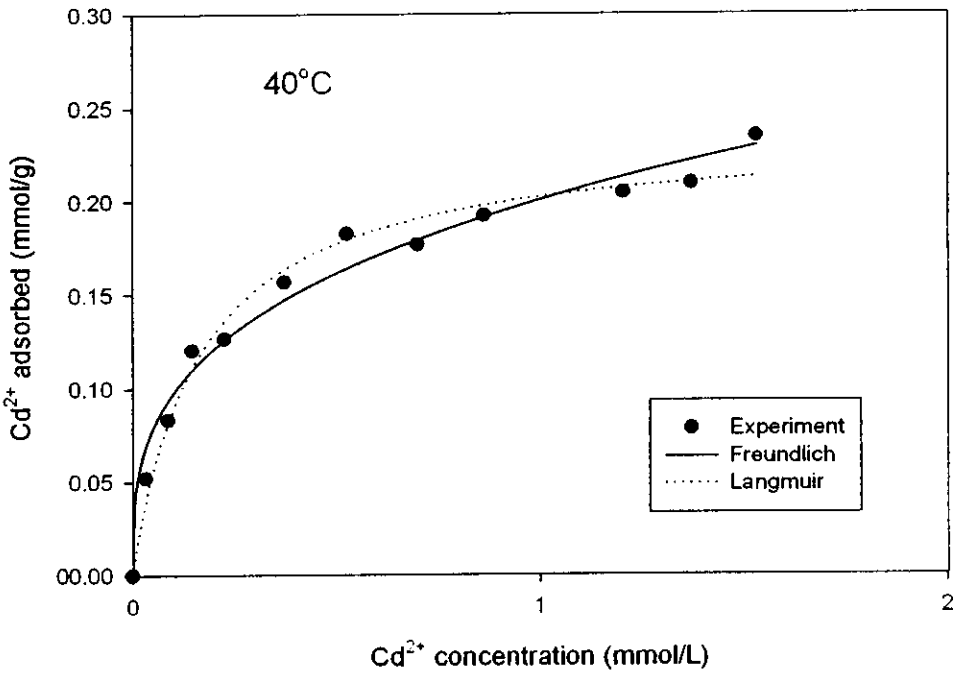

Figure 27 Adsorption isotherm of Cd^{2+} on B-70-600 at temp = 40°C, pH = 5.

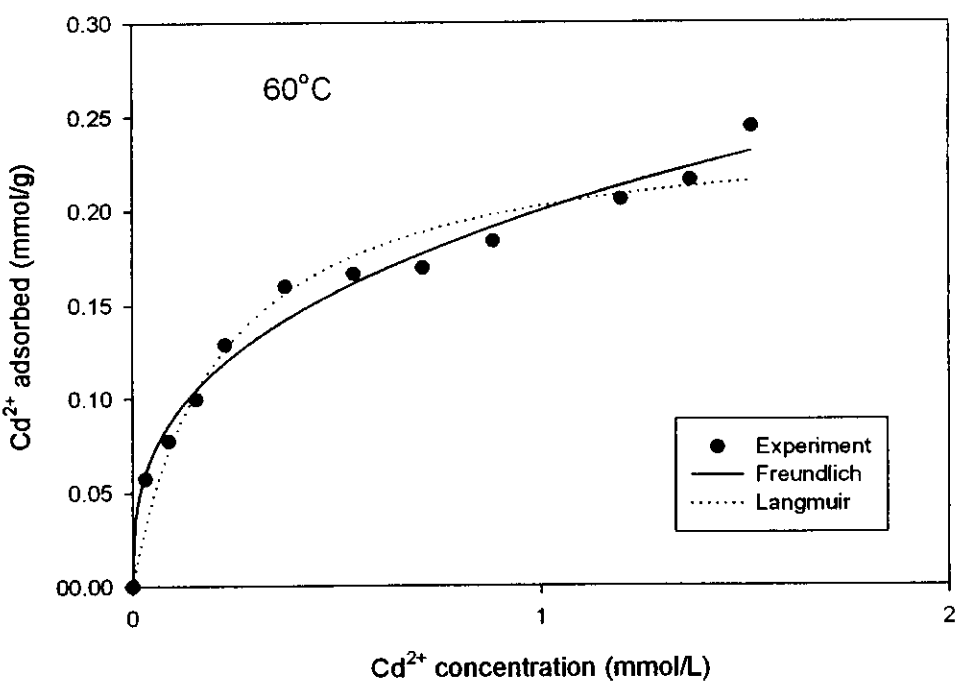

Figure 28 Adsorption isotherm of Cd^{2+} on B-70-600 at temp = 60°C, pH = 5.

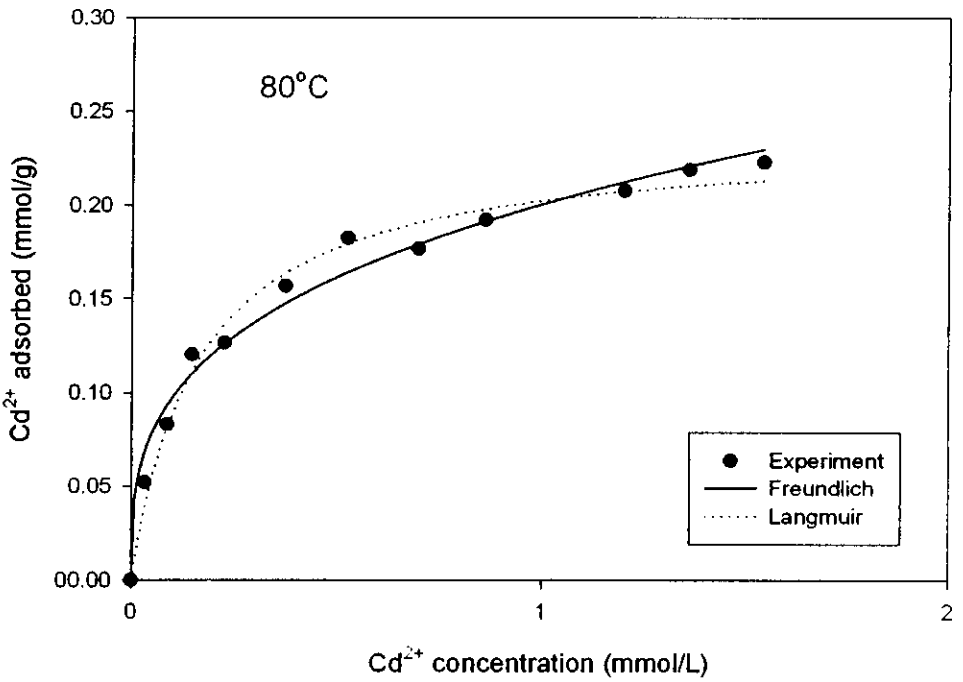

Figure 29 Adsorption isotherm of Cd^{2+} on B-70-600 at temp = 80°C, pH = 5.

Table 7 Parameter values of the Langmuir and Freundlich equations fitted to the experiment of Cd^{2+} adsorption on B-70-600 at different temperatures.

temp	Langmuir			Freundlich		
(°C)	b	Q_m	r^2	K_F	n	r^2
40	6.093	0.2353	0.9798	0.2005	0.313	0.9785
60	4.657	0.2456	0.9609	0.1998	0.3483	0.9835
80	6.094	0.2355	0.9852	0.2006	0.3119	0.9815

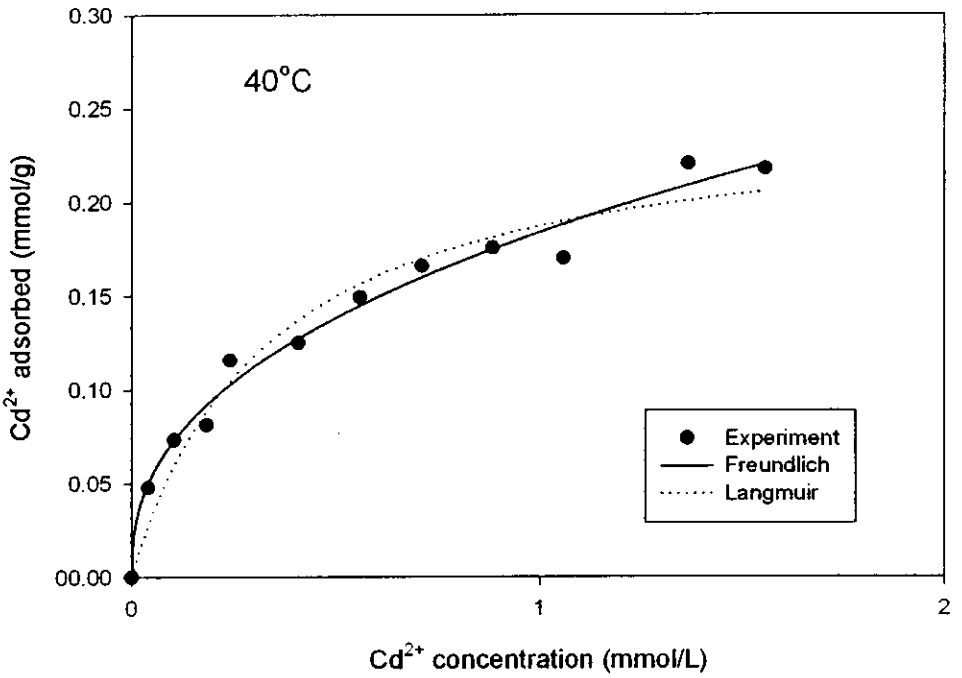

Figure 30 Adsorption isotherm of Cd^{2+} on B-325-800 at temp = 40°C, pH = 5.

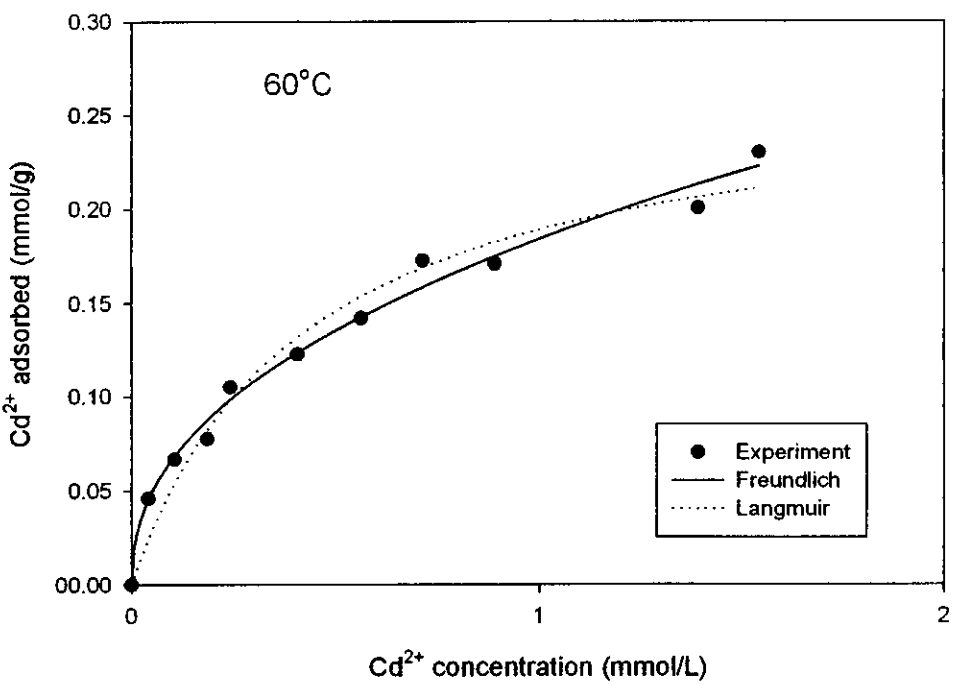

Figure 31 Adsorption isotherm of Cd^{2+} on B-325-800 at temp = 60°C, pH = 5.

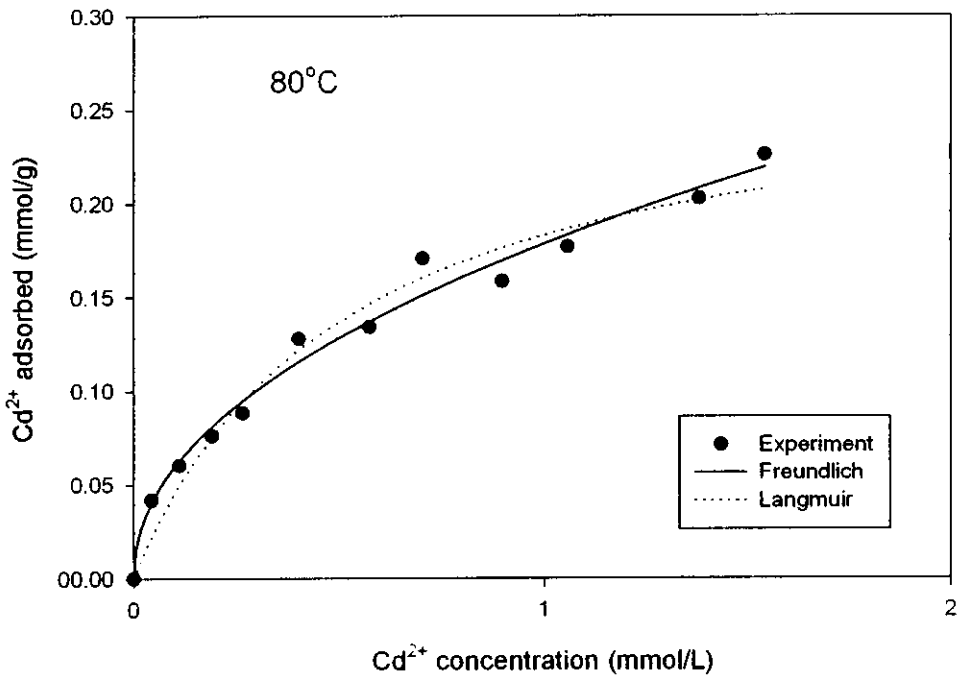

Figure 32 Adsorption isotherm of Cd^{2+} on B-325-800 at temp = 80°C, pH = 5.

Table 8 Parameter values of the Langmuir and Freundlich equations fitted to the experiment of Cd^{2+} adsorption on B-325-800 at different temperatures.

temp	Langmuir			Freundlich		
(°C)	b	Q_m	r^2	K_F	n	r^2
40	3.021	0.2491	0.961	0.1838	0.4067	0.9838
60	2.401	0.2677	0.9698	0.1841	0.4393	0.9882
80	1.965	0.2759	0.9695	0.1783	0.4752	0.9835

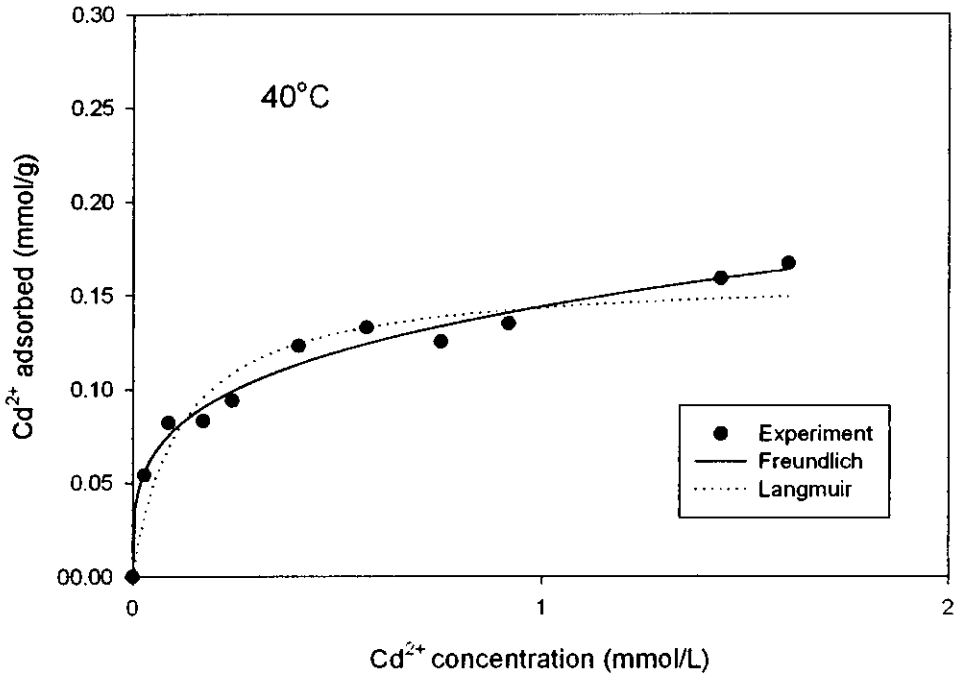

Figure 33 Adsorption isotherm of Cd^{2+} on Pr-70-600 at temp = 40°C, pH = 5.

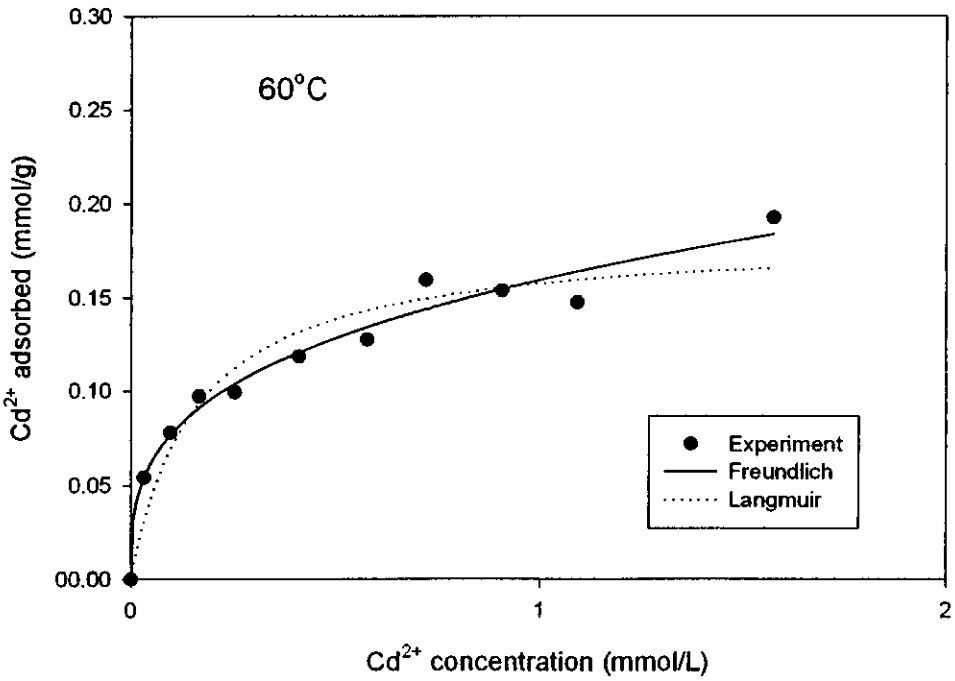

Figure 34 Adsorption isotherm of Cd^{2+} on Pr-70-600 at temp = 60°C, pH = 5.

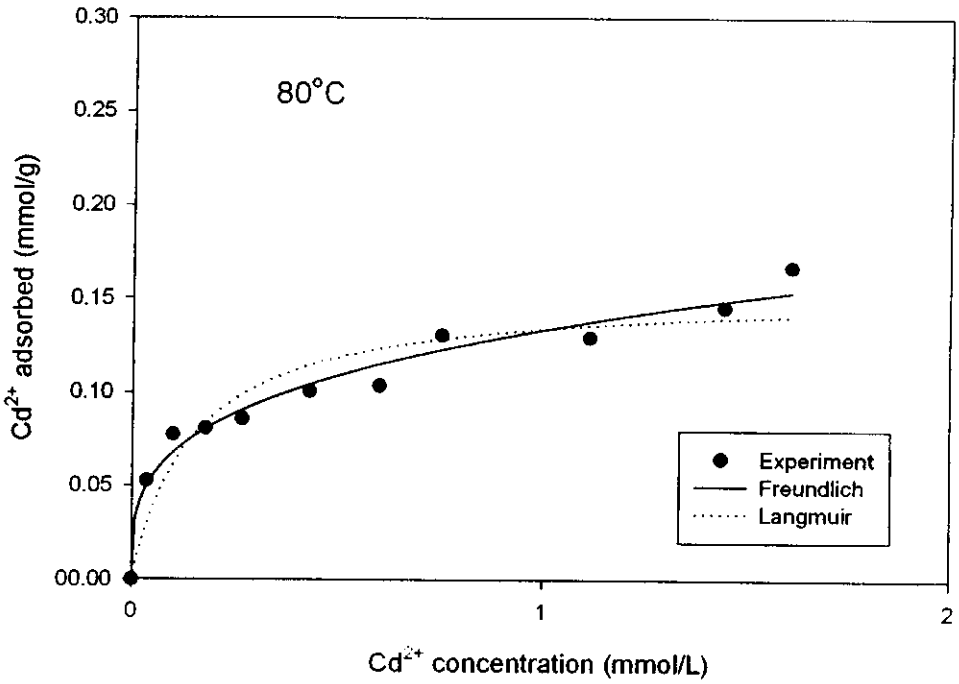

Figure 35 Adsorption isotherm of Cd^{2+} on Pr-70-600 at temp = 80°C, pH = 5.

Table 9 Parameter values of the Langmuir and Freundlich equations fitted to the experiment of Cd^{2+} adsorption on Pr-70-600 at different temperatures.

temp	Langmuir			Freundlich		
(°C)	b	Q_m	r^2	K_F	n	r^2
40	8.521	0.1602	0.9276	0.1441	0.2669	0.9826
60	6.244	0.1827	0.9261	0.1594	0.3139	0.9764
80	6.781	0.1536	0.8932	0.1334	0.2922	0.9727

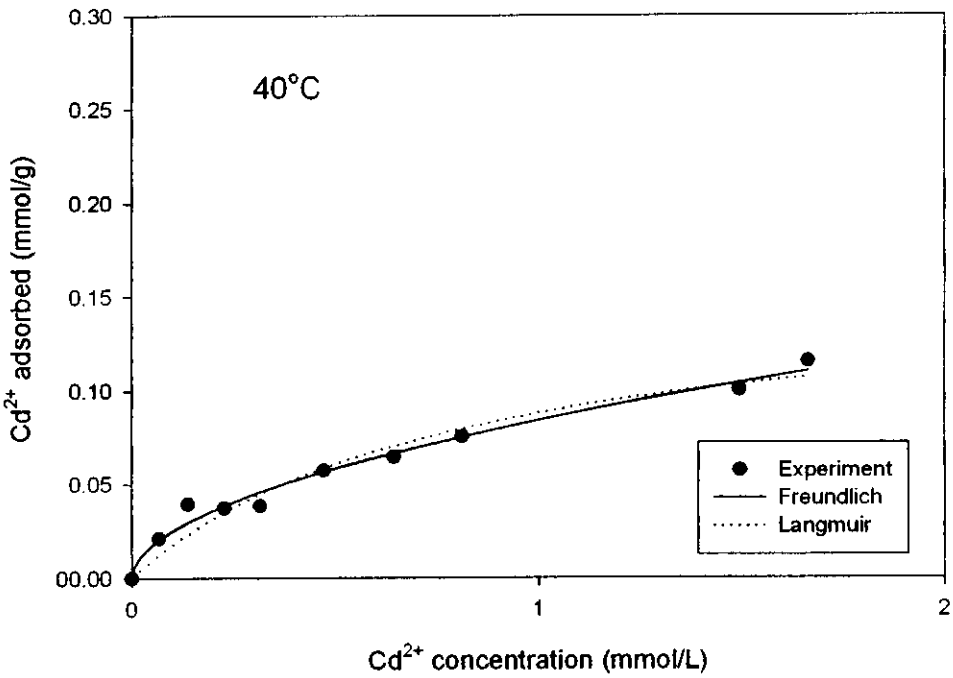

Figure 36 Adsorption isotherm of Cd^{2+} on Pr-325-800 at temp = 40°C, pH = 5.

Table 10 Parameter values of the Langmuir and Freundlich equations fitted to the experiment of Cd^{2+} adsorption on Pr-325-800 at temp = 40°C.

temp	Langmuir			Freundlich		
(°C)	b	Q_m	r^2	K_F	n	r^2
40	1.23	0.1598	0.9547	0.0842	0.5295	0.9825

Adsorption isotherms

Adsorption isotherms of both metal ions on obtained activated carbons which were conducted at initial pH = 5 and at different temperatures are shown in Figure 17 - 36 together with models of adsorption isotherms based on Langmuir and Freundlich.

Adsorption characteristics between the obtained activated carbons and both metal ions (Cd^{2+} and Pb^{2+} ions) can be described by adsorption isotherms. In this work, the Freundlich and Langmuir isotherm have been used for studying the adsorption data. These isotherms relate amounts of metal ions per unit weight of adsorbents (Q, mmol/g) to the equilibrium concentration of metals (C_e, mmol/L). The Langmuir and Freundlich parameters are obtained by using nonlinear regression by fitting the data directly to the equation (1) and (4), respectively (equation (1) and (4) as cited in chapter 1), since algebraic transformation to linear forms (equations (2) and (5)) can negatively influence the estimated constants. The values of parameters of Langmuir and Freundlich equations are summarized in Tables 3 – 10. Also, to compare the reliability of these adsorption isotherms, the correlation coefficient (r^2) for each adsorption isotherm has been calculated and shown together with Langmuir and Freundlich parameters. The correlation coefficient (r^2) is a good criteria and means that the difference between experimental data and theoretical values is small when the values of the coefficient approaches 1 (Bembnowska, et al., 2003).

Based on the values of the correlation coefficients (r^2) for the different isotherm plots, it appears that the adsorption isotherm results of the most of activated carbons for both Pb^{2+} and Cd^{2+} ions can be well described by the

Langmuir equation and the Freundlich equation but the latter gave a slightly better result than the former. From this reason, it is apparent that most of adsorption behavior of both metal ions on obtained activated carbons will be more heterogeneous.

Many researchers have used amounts of metal ions adsorbed at monolayer coverage or well known as maximum adsorption capacities (Q_m, mmol /g) from Langmuir model isotherm to either explain or compare the ability of adsorbate in adsorption (Jia, et al., 1998). In this research, however, we have not chosen this parameter for comparison in our systems. The assumptions of the Langmuir isotherm would be difficult to justify for metal ion adsorption from solution. Therefore, there would be little or no meaning to the analysis of the ability of adsorption. Also, it is sometimes not suitable to relate the success of a model to the mechanism assumed by this model because it is always possible to find a deterministic or statistic model which fits experimental data.

Although parameters from Langmuir model cannot explain the behavior of all systems as be homogeneous well, Freundlich may be better used for adsorption behavior.

The Freundlich equation is of the form

$$Q = K_F \cdot C^n \qquad \text{(nonlinear form)} \quad (4)$$

where K_F is the so-called unit capacity factor which shows adsorption capacity and n (dimensionless) is the empirical parameter that represents the heterogeneity of the site energies and also is the indicative of the intensity of adsorption. Both K_F and n can be maximum values as 1 which will show severe adsorption capacity. Moreover, it will be apparent heterogeneity due to

several forms of binding site for adsorption process. Consideration of *n*, *n* values are around 0.2-0.3 for adsorption of all activated carbons toward Pb^{2+} whereas around 0.3-0.5 toward Cd^{2+}. These values reflect the less heterogeneity of activated carbons toward both metal ions.

Considerably, effect of temperatures to metal ions adsorption of each activated carbon does not affect the adsorption isotherm as show the overlapping in the graph and similar Langmuir and Freundlich parameters at various temperatures. This problem will be mentioned again in thermodynamic considerations.

Comparison of adsorption capacity.

Adsorption capacities become suitably to be used for comparison of the ability of each activated carbon due to unclearness of Langmuir and Freundlich models. As can be observed by comparison in Figures 17- 36, the order of adsorption capacities over entire range of studies are in the following: B-70-600 > B-325-800 ≈ Pr-70-600 > Pr-325-800 for Pb^{2+} adsorption and B-70-600 ≈ B-325-800 > Pr-70-600 > Pr-325-800 for Cd^{2+} at the same initial pH (pH =5) and temperatures. We can imagine that in the case of the high ionic radius of Pb^{2+}, the result may be explained in terms of pore accessibility (Kadirvalu, et al., 2000). In the case of Pr-70-600 and Pr-325-800 (micropore activated carbons), some micropore entrances may be blocked by hydrolyzed *metal species which are larger than the metal ions. Accordingly, surface groups located in micropores are no longer accessible and some surface sites* are not used for adsorption. In the case of B-70-600 and B-325-800, which contain more mesopores, accessibility to micro- and mesopores is not blocked by hydrolyzed species and almost surface sites can be used for

adsorption of lead ions. In addition, acidity of surface becomes another factor to define adsorption capacities (Ferro-Garcy, et al., 1998). Activated carbons which have lower pH_{pzc} values should have more adsorption capacities than the higher. Therefore, it is unequivocal to support the highest adsorption of Pb^{2+} on B-70-600 which has both the highest mesopore and lowest pH_{pzc} value. Although B-325-800 is mesoporous carbon but adsorption capacity toward Pb^{2+} resembles to Pr-70-600 which less mesopore contents due to Pr-70-600 have lower pH_{pzc}. Pr-70-600 has both the lowest pH_{pzc} and mesopore content so, it shows the lowest adsorption capacity toward Pb^{2+}.

For Cd^{2+} adsorptions for all activated carbons are not same to Pb^{2+} adsorption. The adsorption capacities of B-70-600 resemble to B-325-800 and Pr-70-600 resemble to Pr-325-800. These results may be elucidate by porous texture than by pH_{pzc} due to Cd^{2+} have the low electronegativity which is weaker attractive force compared to Pb^{2+}(McQuarrie, 1991). Similarities in porous characteristics can be determined the adsorption capacities of each samples. However, the reasons which give more understanding in adsorption capacities between Cd^{2+} and those activated carbons which have the same or near pH_{pzc} values but difference in porous textures remain many debates (Savoka, et al., 2003).

Thermodynamic Considerations.

From the previous study, some general conclusions can be deduced regarding the energetic changes occurring during the process. Thus, the *b* parameter from Langmuir equation can be related to the enthalpy or heat of adsorption (ΔH_{ads}) as follows (Adamson and Gast, 1997)

$$b = b' e^{(\Delta H_{ads}/RT)} \qquad (3)$$

this equation is so called van't Hoff equation, where R is the universal gas constant (8.314 J K^{-1} mol^{-1}), T is the temperature in Kelvin and b' is pre-exponential factor constant. If the isotherm of adsorption can be fitted with Langmuir model adequately, the heat of adsorption process at monolayer coverage can be investigated from equation (3).

For Freundlich model, there is another propose that usually be used to explain heat of adsorption. Isothermal data obtained at three different temperatures (40, 60 and 80°C) are used to estimate the isosteric heat of the process. Consequently, enthalpy changes associated with adsorption processes can be estimated using the Clausius-Clapeyron equation. In this way, the isosteric heats of adsorption, ΔH_{ads}, for various loadings (or amounts adsorbed) are calculated from equation (6) by means of the isosteres corresponding to each amount adsorbed

$$\left(\frac{d\ln C_e}{dT}\right)_Q = \frac{\Delta H_{ads}}{RT^2} \qquad (6)$$

or

$$\Delta H_{ads} = -R\left[\frac{d\ln C_e}{d(1/T)}\right]_Q \qquad (7)$$

In equation (6) and (7), ΔH_{ads} is the isosteric heat of adsorption (kJ mol^{-1}), a measure of the enthalpy change involved in the transfer of solute from the reference state to the adsorbed state at a constant solid-phase concentration; C_e and Q are the equilibrium aqueous-phase and solid-phase concentrations,

respectively; R is the universal gas constant (8.314 J $K^{-1}mol^{-1}$), and T is the temperature in Kelvin.

Aqueous-phase solute concentrations (C_e) at three different temperatures are calculated at constant solid-phase solute concentration (Q) using the calculated isotherm parameters. A linear regression of ln C_e as a function of $1/T$ yields a single value of ΔH_{ads} and its coefficent of determination at a given Q.

From knowledge of Clausius-Clapyron equation, it is expected to employ this equation for considering behavior of adsorption to be either heterogeneity or homogeneity process (Adamson and Gast, 1997). If the resulting values of ΔH_{ads} for any activated carbon are almost constant regardless of the amount adsorbed in the interval of Q examined, these results suggest that those activated carbons exhibit an energetically homogeneous surface. In contrast, if the isosteric heat values for adsorption are found to vary as coverage increased, they will be exhibited typical of energetically heterogeneous surfaces. Variations in the isosteric heat of adsorption with surface coverage have been postulated to result from heterogeneous sorption energies due to the differences in sorbate lateral interactions, particle geometry, and interaction energies among sites on edge basal surfaces.

Nevertheless, both equation (3) and (6) cannot be possible to calculate the isosteric heat of adsorption of both metal ions for all activated carbons (except Pr-325-800 due to no observation) because the equilibrium concentration did not increase or decrease monotonically with increasing temperature. In the other hand, adsorption of both ions cannot be affected by temperatures which cannot be determined thermodynamic parameters. This can be explained if chemical interactions between the metal ions and the

surface of this particular carbon occurred to some extent, overwhelming physical interactions. This problem is too complicated to solve.

Noticeably, the extents of adsorption of ions or molecules have been found to increase with temperature (Singh, et al., 2003), indicating the process to be endothermic in nature. The increase in the uptake of ions or molecules with temperature may be due to the enhanced rate of intraparticle diffusion of the adsorbate because the diffusion is an endothermic process. The increase in the adsorption behavior suggests that active surface centers available for adsorption have increased with temperature. An increasing number of ions or molecules may also acquire sufficient energy to undergo an interaction with active sites at the surface. This evidence may contrast to some scientists who think that heat of adsorption can be exothermic process exclusively. This may be always true when considering in adsorption in gas phase but in the solution phase, especially aqueous solution, heat of adsorption can be either exothermic or endothermic process.

Approach of the Adsorption Mechanism.

To understand the adsorption mechanism of metal ions by activated carbon, the effect of pH was studied. First, the final values of pH at adsorption equilibrium were measured, for an initial pH of 5, for each isotherm by comparison of the metal ions adsorption studies with the corresponding blank reference studies. Results of measurements have shown that for all activated carbons and for all initial metal concentrations, the final pH was higher than initial pH. The final pH decreased when the initial metal concentration increased. The decrease of pH when initial metal concentration increases may be due to the release of H^+ ions and may indicate an adsorption mechanism

by ion-exchange (Jia, et al., 2000 and Kadirvalu, 2000). The release of protons from carbon when contacting with metals solutions were entirely ascribed to the adsorption of metal ions which displaced the protons from the carbon surface. The ion-exchange mechanism between H^+ ions at the activated carbon surface and metal ions may happen following these reactions:

$$2\ \text{S-COH} + M^{2+} \leftrightarrow \text{S-(CO)}_2M^{2+} + 2H^+$$

$$\text{S-COH}_2^{2+} + M^{2+} \leftrightarrow \text{S-COM}^{2+} + 2H^+$$

This result is corresponding to FT-IR results which have shown absorption bands of acidic surface oxide on all activated carbon samples. These surface oxides can reveal properties in exchanging between proton and metal ions in aqueous solution. Also, it is possible that these above mechanisms are not affected by temperature change so the heat of adsorption (ΔH_{ads}) cannot be calculated (Anderson and Rubin, 1981 and Cheremisinoff, 1978).

Soxhlet extraction with water was also used to remove reversible metal ions adsorbed from activated carbon surface. It is apparent that there have been metal ions in residual solutions after washing process (analyzed by AAS) but they are very little amounts. Therefore, it is possible to conclude that most of metal ions are adsorbed on activated carbon surface irreversibly (strong chemical bonding). This was confirmed by EDA studies of the surface of all activated carbon after adsorption of both metal ions at pH=5 and temperature = 40°C followed by Soxhlet extraction with water. The EDA results in Figure 37 - 40 are demonstrated the presence of metal ions which irreversibly adsorbed

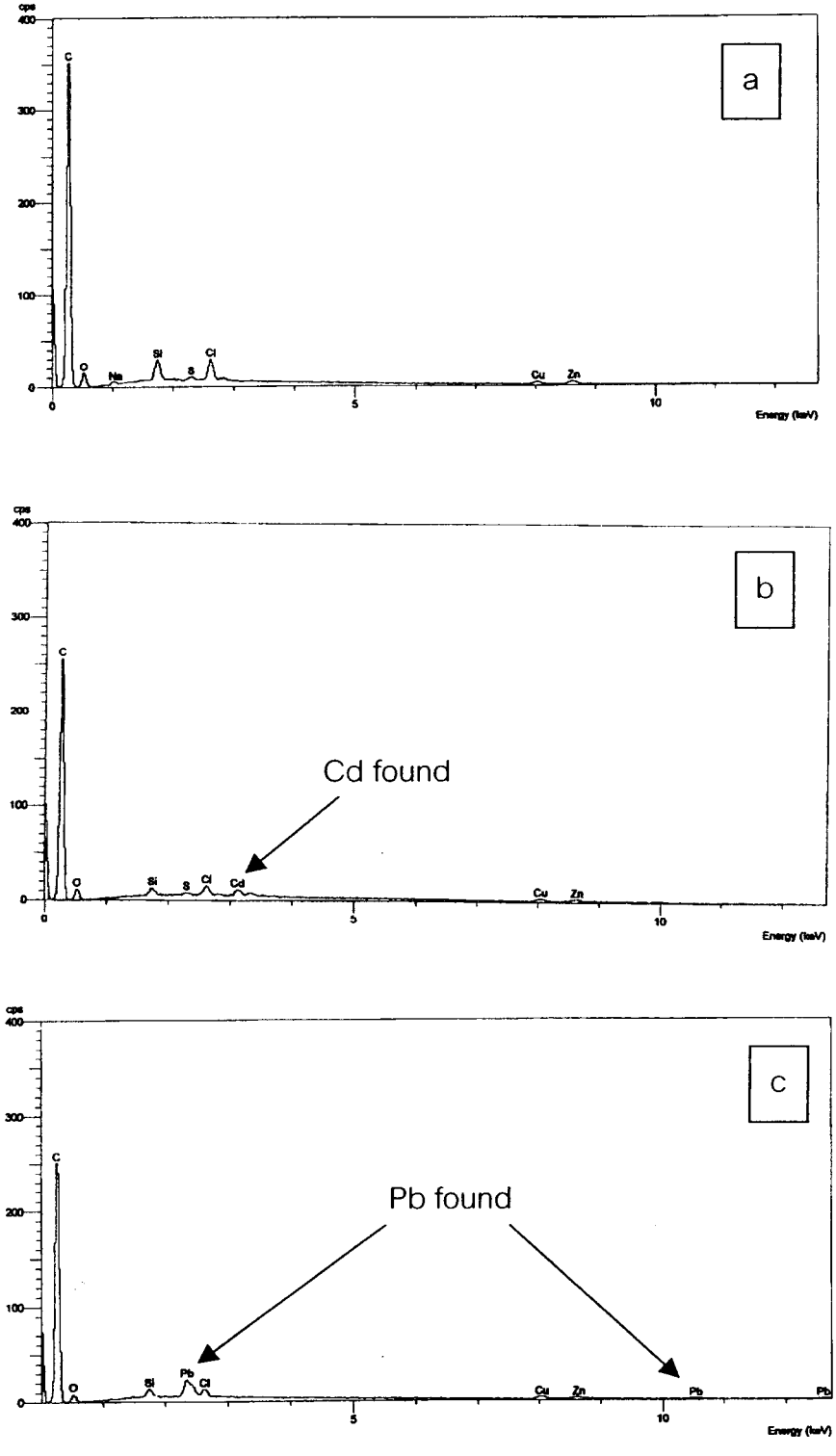

Figure 37 EDA spectrometry of B-70-600 (a), B-70-600/Cd^{2+} (b) and B-70-600/Pb^{2+} (c).

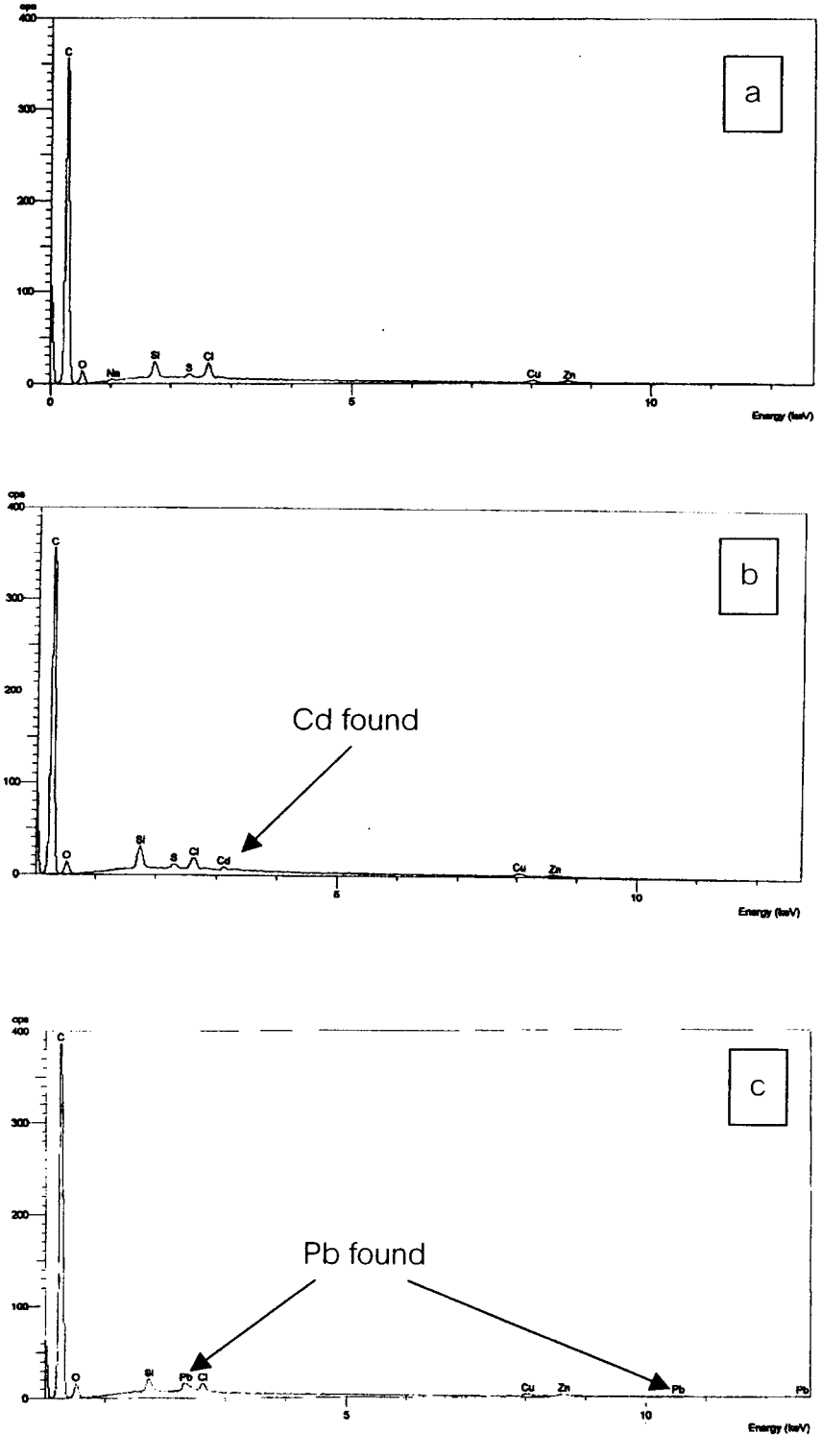

Figure 38 EDA spectrometry of B-325-800 (a), B-325-800/Cd^{2+} (b) and B-325-800/Pb^{2+} (c).

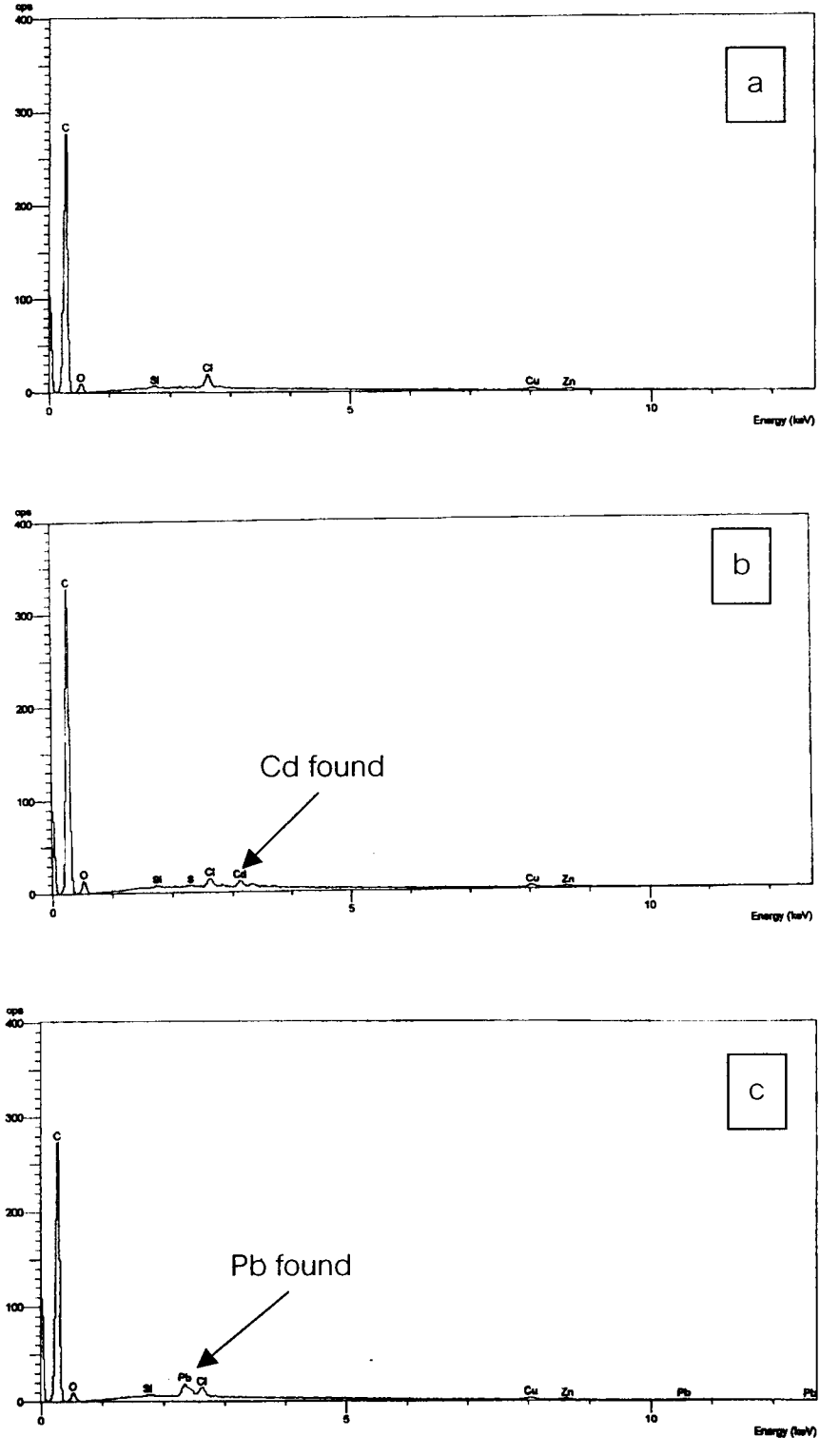

Figure 39 EDA spectrometry of Pr-70-600 (a), Pr-70-600/Cd^{2+} (b) and Pr-70-600/Pb^{2+} (c).

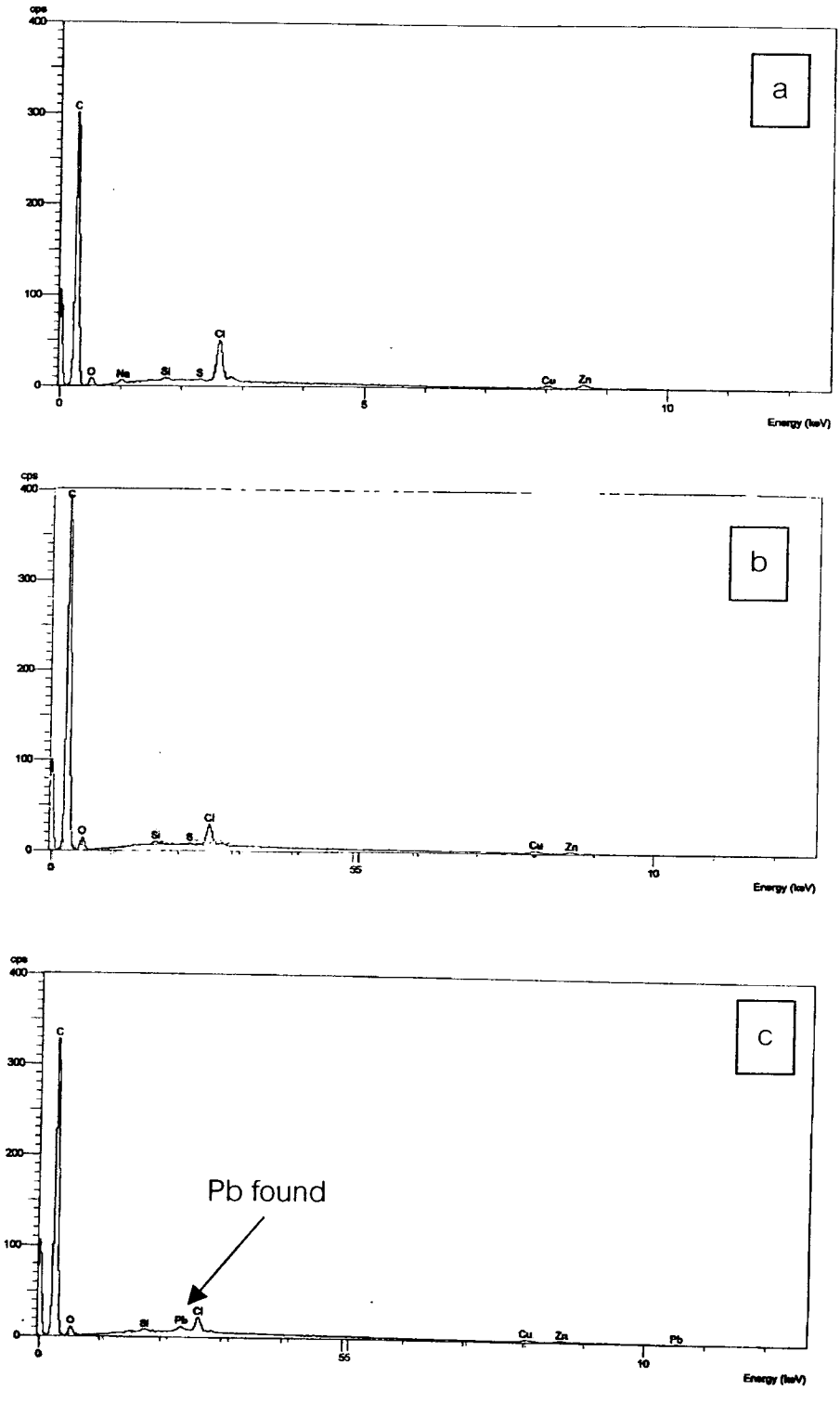

Figure 40 EDA spectrometry of Pr-325-800 (a), Pr-325-800/Cd^{2+} (b) and Pr-325-800/Pb^{2+} (c).

by all samples except Pr-325-800 which did not have cadmium ions after washing process.

The presence of metal ions both on activated carbon surfaces and in residual solution after washing can confirm adsorption behavior as heterogeneity. Metal ions adsorbed on activated carbon are attached by chemical bonding due to ion-exchange process whereas another which washed out by water are weaker attach by electrostatic or van de Waal interactions. It is reasonable to conclude that both ion-exchange and such weaker interaction may involve in adsorption process but ion-exchange show more attractive compare to weaker interaction. This explanation is corresponding to the adsorption isotherms which obey Freundlich more than Langmuir.